Orbital forcing of African hydroclimate over the past 800,000 years

Edward Armstrong

edward.armstrong@helsinki.fi

University of Helsinki

Miikka Tallavaara

University of Helsinki https://orcid.org/0000-0001-9252-7309

Sakari Salonen

University of Helsinki https://orcid.org/0000-0002-8847-9081

Jon Camuera

Andalusian Earth Sciences Institute (IACT), Spanish National Research Council (CSIC)
https://orcid.org/0000-0002-6799-7269

Rahab Kinyanjui

MPI-SHH https://orcid.org/0000-0003-2032-8321

Paul Valdes

Bristol University https://orcid.org/0000-0002-1902-3283

Article

Keywords:

Posted Date: September 5th, 2024

DOI: https://doi.org/10.21203/rs.3.rs-4984955/v1

Additional Declarations: There is **NO** Competing Interest.

Abstract

The African hydroclimate played a key role in shaping the evolutionary environment of numerous species including hominins. African precipitation is sensitive to insolation and is consequently strongly linked to Earth's orbital variations. Here, we utilise singular spectrum analysis to extract key orbital frequencies from a range of proxy records and a climate model dataset generated using the HadCM3B-V1.0 model, to reveal key patterns of pan-African orbital forcing of hydroclimate variability over the past 800,000 years. The model and proxies show good agreement. Eccentricity modulated precession forcing is the dominant mode of variability in both proxies and model, driving enhanced summer monsoon precipitation across a North-South interhemispheric antiphase. The impact of eccentricity is complex and associated with precession modulation, direct insolation change, and indirect feedbacks linked to greenhouse gases and ice-sheet extent. Obliquity primarily influences the amplitude of precession forcing. Our results suggest that the combination of different orbital forcings created complex spatio-temporal precipitation patterns, and consequent ecosystem dynamics in Africa.

Key Points

Palaeoclimatology, African climate, climate dynamics, hominin evolution, human evolution, human dispersal, orbital cycles, Milankovitch cycles, climate forcing, climate feedbacks, monsoons.

Introduction

Climate is coupled to insolation. Consequently, a key driver of Quaternary palaeoclimate variability is understood to be changes in orbital parameters[1–5]. Africa's palaeoclimate is a fundamental factor governing the evolution and dispersal of species including ancient humans[6–10]. Therefore, hominin biogeography and evolution has been strongly linked to orbital forcing of African climate and particularly its hydroclimate, as precipitation regulates vegetation and productivity which determines hominin habitat suitability[11–13].

Contemporary precipitation in Africa is driven predominantly by convection associated with the Hadley Circulation, tropical rain belt, monsoon system, and the Intertropical convergence zone (ITCZ), which migrates seasonally across the Equator into the warmer hemisphere[14]. The descending branches of the Hadley Cells inhibit convection over the Sahara and South Africa, generating arid regions in the North and South of the continent. In Eastern Africa there is an atypical equatorial semi-arid hydroclimate, with rainfall influenced by the East African Rift valley topography and the dynamics of the Walker Circulation. The three ocean basins that surround the continent also influence precipitation at different spatial and temporal scales[15,16].

The quasi-regular cycles of eccentricity, obliquity and precession influence the amount of solar radiation, its latitudinal distribution which influences seasonal intensity, and its seasonal distribution which determines the season which receives enhanced insolation, respectively[17–20]. Obliquity has a periodicity of ~ 41 kyr and influences the distribution of insolation at different latitudes, with high latitudes affected the most. In contrast, low-latitude insolation and seasonality is primarily affected by precession, which drives warmer summers and concurrent colder winters with a periodicity of ~ 21 kyr. Eccentricity, which has periodicities of ~ 100 kyr and ~ 400 kyr, acts as a modulator of precession and therefore of low latitude forcing. Additionally, its regulation of insolation has driven the high-latitude glacial-interglacial ice-sheet phases and variations in greenhouse gas concentrations over the past 800 kyrs, which may also indirectly influence low-latitude African palaeoclimate[18,19,21,22]. The impact of eccentricity is therefore complex and multi-faceted.

Recently, it has been suggested that the predominant source of long-term environmental change in Africa was the opposing wet-dry states in eastern and western Africa caused by 400kyr-eccentricity driven shifts in the Walker Circulation[23,24]. From a thermodynamic perspective however, African climate should respond primarily to eccentricity modulated precession forcing as this is the primary control on low latitude insolation[17]. Indeed, numerous observations from across Africa demonstrate precession forcing, including the North African Humid Periods (NAHPs)[25–30]. However, although its direct influence appears straightforward, its imprint may be influenced by obliquity and eccentricity forcing[21,31]. These cycles are also evident in observations[1,32,33], and complicate low-latitude precession influence via ocean and atmospheric feedbacks[21,22,31,34]. It is evident, therefore, that the climatic influence of orbital forcing in Africa is complex and spatially heterogenous, and it is important to derive a better understanding of its impact on Africa's palaeo-hydroclimate.

In this study, we aim to consolidate our current understanding of the role of orbital forcing in pan-African hydroclimate variability over the past 800kyr. We will do this by comparing and combining information from long-term proxy data, including five new pollen-based precipitation reconstructions, and a complex coupled climate model dataset generated using snapshot simulations (see Methods). Proxy records provide the primary source of information of African moisture availability, but deriving a coherent understanding of orbital forcing is restricted by the paucity, uncertainty, and limited temporal and spatial resolution of these records. Climate models can be used to complement the information derived from proxies. However, computational limitations associated with the extensive run times required have limited such analysis. Furthermore, models have been shown to be too stable, as shown by the inability of models to simulate the NAHPs with adequate magnitude[35,36]. Crucially our model simulates the NAHPs with comparable amplitude to observations[34,37], therefore demonstrating a more realistic hydroclimate response to precession when compared to many other models[34,35]. Our approach of combining information from proxies and climate model permits us to explore how strongly the spatio-temporal variation in hydroclimate is related to orbital forcing, what are the major modes and mechanisms of spatial and temporal variability including distinguishing the role of direct insolation and high latitude feedbacks, and how well the data support recent hypothesis regarding main modes of

precipitation variability. Furthermore, proxy-model comparisons highlight the potential areas of uncertainty (disagreement between different sources of information) in our knowledge that require further exploration.

Our results show that proxies and model are broadly in good agreement. Precession is the dominant forcing of pan-African hydroclimate variability, characterised by an inter-hemispheric antiphase, with minimum (maximum) precession enhancing North (South) African annual precipitation. Obliquity drives an equatorial-subequatorial antiphase, and the model indicates its primary influence is to enhance precession forcing. Eccentricity is complex and associated with three mechanisms; the modulation of precession, its direct influence on insolation, and the indirect feedbacks associated with greenhouse gas and ice-sheet forcing. Broadly it drives a similar spatial imprint to precession, with high (low) eccentricity enhancing North (South) African rainfall. However, its primary impact is also to modulate the amplitude of precession variability. The combination of these drivers produces complex spatio-temporal climate patterns that can result in interesting ecosystem dynamics in Africa.

Results

Observed and modelled pan-African hydroclimate variability

To evaluate our current understanding of orbital variability we have analysed 17 moisture proxy records from across Africa, selected due to their long temporal duration (> 150kyr), resolution, and wide spatial coverage. The proxies are summarised in Table 1, Fig. 1a, Supplementary Fig. 1 and the Methods.

To complement the analysis of proxy data, we utilise a climate model reconstruction spanning the past 800kyr produced using the HadCM3BB-v1.0 climate model[34,37,38]. The dataset has been generated using 219 snapshot simulations, each incorporating varying orbital parameters, ice-sheet extent, and greenhouse gas concentrations (GHGc; Supplementary Fig. 6; Methods). The model has been validated in Armstrong, et al. [34] and shown to accurately simulate present-day African precipitation and wind patterns, and produces an 800-kyr climatology that is in agreement with Quaternary proxies of SATs, SSTs and precipitation (see also Supplementary Fig. 1).

Figure 1b-c shows modelled African annual precipitation averaged over the past 800kyr and its standard deviation (mm/yr). African precipitation is dominated by convection in the tropics, in the region between the boreal and austral summer rainbelt. Precipitation variability is greatest in North Africa between 5°-25°N, in the location of the boreal summer (JJA) rainbelt and West African Monsoon (WAM) system. Variability is most stable in Northeast, central and Southern Africa.

To identify coherent oscillations that demonstrate orbital frequencies within the proxy data and model, we utilise singular spectrum analysis (SSA, Methods)[39–41]. SSA decomposes a timeseries into its oscillatory components, from which we extract and reconstruct the orbital frequencies. The de-trended proxy timeseries, and corresponding SSA-extracted orbital component timeseries that are 75% confident

relative to a stochastic (Markov) process (Methods) are shown in Supplementary Fig. 2 (see also Supplementary Fig. 5). Figure 1d-g show the variance contribution (%) of each orbital component to the overall proxy and model timeseries variance. Proxy components are shown as filled circles where 75% confident, and are summarised in Table 1. African regions discussed throughout the text are defined in Fig. 1a and the Methods.

Orbital frequencies (at 75% confidence) comprise between 21–70% of the proxy timeseries variance (Table 1), with an average of 45%. This demonstrates that orbital forcing is a significant driver of observed African moisture variability over the mid-late Quaternary. In the model, the combined orbital frequencies comprise approximately 95+% of precipitation variability. This reflects the model forcings (orbital parameters, ice-sheets and GHGc; Supplementary Fig. 6) which fluctuate on orbital timescales, with no additional internal noise.

Precession is the dominant forcing of hydroclimate variability over the past 800kyrs in both proxy and model data. Each proxy demonstrates significant 21kyr precession frequencies (Fig. 1g, Supplementary Fig. 2), accounting for on average 30% of the variance. This constitutes the majority of orbital variance for most observations. In the model, precession accounts for an average 73% of total variability. Eccentricity accounts for on average 15% of the variance in the four proxies it is statistically significant, and in the model up to 25% variance in Central Africa. The proxy, model and SSA-decomposed precession timeseries (Fig. 3; Supplementary Figs. 1, 2, 5) also demonstrate precession modulation by 100kyr eccentricity in both Northern (NH) and Southern Hemisphere (SH) proxies. In the model, 400kyr-eccentricity modulation is also evident (Fig. 3, Supplementary Fig. 5). At high eccentricity there is enhanced precession forcing, and therefore larger differences in precipitation between precession minima and maxima phases. Despite Africa's low latitude location, obliquity frequencies are evident in many of the proxies (Fig. 1f, Table 1) accounting for 16% of average variance, indicating that it has a significant influence on Africa's hydroclimate. It broadly contributes more to observations in Central and East Africa. In the model, obliquity accounts for up to 40% of variability in Central Africa and 20% in Southeast and North Africa.

To analyse the spatial patterning related to different orbital forcings, we have calculated the average moisture difference between high/maximum minus low/minimum orbital phases (Fig. 1h-k). For the proxies, solid colours are 75% confident and calculated from the orbital component timeseries, whereas crossed opaque colours are not confident signals and calculated directly from the proxy timeseries (see Methods). Orbital periods are defined by the blue and red phases in Supplementary Fig. 3.

The spatial impact of precession is a North-South interhemispheric antiphase (Fig. 1k), which is a robust feature in both proxies and model. Precession minima (enhanced Northern Hemisphere summer insolation) is associated with enhanced moisture availability in North Africa (~ 140mm/year; Figs. 1k, 3a). In contrast, proxies and model in South, East and West Africa indicate enhanced moisture (~ 58mm/year) at precession maxima (enhanced Southern Hemisphere summer insolation). In Central

Africa, modelled precession forcing is weaker, consistent with Con2 but not Con1 (19% and 56% variance explained by precession respectively).

The proxies and model indicate that periods of high (low) 100-kyr eccentricity are characterised by a wetter (drier) North and Central Africa, and drier (wetter) southern subequatorial Africa (Fig. 1i). The spatial imprint is a North–South antiphase, similar to precession. Problematically 75% confident signals are identified in only 4 records (BOS, Lim2, Mal2 and CBH; Fig. 1d, h). Furthermore, the model indicates drier (wetter) conditions at high (low) eccentricity in East Africa in agreement with Mal1, but contrary to Mal2 and Koora. In the Limpopo Basin, there is also discrepancy as Lim1 indicates wetter (drier) high (low) eccentricity whilst Lim2 suggests an opposing pattern. However, the model indicates this basin straddles a regional antiphase, so differences between proxies may reflect varied source region and/or transport pathways. The eccentricity modulation of precession increases (decreases) variability during high (low) eccentricity, which is overprinted on these high (low) eccentricity phases (e.g. Supplementary Fig. 2k).

Modelled 400-kyr eccentricity accounts for only a small amount of variance (Fig. 1d) and is characterised by a Southeast-Northwest antiphase (Fig. 1h). High (low) eccentricity is associated with drier (wetter) conditions in West, Central and South Africa (1.7mm/year; Fig. 3), and wetter conditions in North and East Africa (4.4mm/year). Spatially, the proxies agree in North, West and East Africa, however there is disagreement in Central and South Africa. Problematically, 75% confident signals are not identified in any observation.

The spatial imprint of obliquity is broadly an equatorial-subequatorial antiphase (Fig. 1j). Periods of high (low) obliquity are associated with increased (decreased) rainfall in subequatorial Africa poleward of 5°N and 12°S by 36.2mm/year in North Africa, and decreased (increased) rainfall in southern Southeast Africa and equatorial Africa by ~ 125mm/yr. There is broadly good proxy-model agreement in North, East, Southeast and Southwest Africa. However, in West and Central Africa there is regional inter-proxy disagreement.

Mechanisms of modelled orbital forcing

To identify the mechanisms of orbital forcing, including isolating the direct insolation effects from the indirect impacts of GHGc and ice-sheet forcing, we have performed additional sensitivity experiments (Methods). A detailed analysis of these and exploration of the orbital mechanisms is provided in the Supplementary Information and a brief overview provided here. The modelled orbital anomalies (precipitation difference between high-low phases) and associated key forcing mechanisms are summarised in Fig. 2. The average regional modelled precipitation anomalies associated with each orbital cycle phase are summarised in Fig. 3a.

Precession

The sensitivity experiments demonstrate that precession forcing is driven primarily by insolation change (Supplementary Fig. 7), with precipitation increasing in the Hemisphere in which summer occurs during

the perihelion. Enhanced summer insolation strengthens the Hadley Circulation in the summer hemisphere, intensifying convection, the rainbelt and monsoon (Supplementary Figs. 8 and 9). As subequatorial rainfall is dominated by these summer convective systems, enhanced summer insolation has a greater impact than the decreased winter insolation. This highlights a non-linear response to altered seasonal insolation, giving rise to an annual-mean precipitation response. In contrast, weak forcing in Central Africa reflects the year-round nature of regional precipitation, resulting in enhanced summer precipitation being balanced by reduced winter precipitation, i.e. a linear hydroclimate response. This occurs during both precession minima and maxima, resulting in minimal annual change.

East African precipitation is coupled to Indian Ocean sea-surface temperatures (SSTs) and the strength of the Indian Ocean Walker Circulation (IWC)[16,42]. The model indicates that precession influences the strength of the IWC (Supplementary Fig. 10) in response to differential heating in the East and West Indian Ocean (Supplementary Fig. 11). At precession maxima (minima), greater (weaker) warming in the West slows (accelerates) the IWC and decreases (increases) convergence over East Africa. This enhances (supresses) convective rainfall, analogous to a positive (negative) Indian Ocean dipole (IOD) mode. In the tip of West Africa, enhanced (reduced) precipitation occurs at precession maxima (minima) due to a northward (southward) shift in the boreal winter ITCZ (Supplementary Fig. 8).

At high eccentricity there is enhanced precession everywhere during both phases (Supplementary Fig. 4). In North Africa, precession amplitude is also influenced by 100-kyr eccentricity controlled ice-sheet forcing, indicating a high-latitude control[34]. At low 100kyr eccentricity (glacials), ice-sheet albedo-driven colder temperatures suppress precession minima amplitude. This results in a greater contrast between high and low eccentricity precession forcing in the NH compared the SH.

Eccentricity

Our model demonstrates that eccentricity influences African precipitation via three mechanisms; its modulation of precession, its direct influence on insolation, and the indirect impact of 100kyr-eccentricity on ice-sheet extent, GHGc and the associated feedbacks.

The sensitivity experiments show the impact of 400kyr-eccentricity is driven by insolation change (Fig. 1h, Supplementary Fig. 7g). At high (low) eccentricity, warmer (colder) temperatures weaken (strengthen) the Hadley Circulation (Supplementary Figs. 12 and 13), decreasing (increasing) divergence and rainfall in Southern Africa. This shifts the rainbelt poleward (equatorward), reducing (increasing) West African rainfall, and decreasing (increasing) subsidence and aridity in North and East Africa. This insolation-only anomaly is comparable for both 400kyr and 100kyr cycles (Supplementary Fig. 7g-h).

The experiments indicate that ice-sheet and GHGc forcings alter the 100kyr-eccentricity insolation response in different ways. GHGc reinforces the Hadley Circulation anomalies, due to its positive feedback on temperatures. It also forces a different regime in the southern half of Southeast Africa, driving wetter (drier) conditions at high (low) eccentricity (Supplementary Fig. 7r). This is linked to SST variations in the Agulhas Current, which feeds the Indian Ocean Southeasterlies (Supplementary Fig. 14).

At high (low) 100kyr-eccentricity, elevated (lower) GHG concentrations further warm (cool) temperatures, which shifts the Southern Subtropical Front (STF) poleward (equatorward) (Supplementary Fig. 15), resulting in a warmer (colder) Agulhas Current, enhancing (reducing) precipitation.

Ice-sheets impact climate via thermodynamic and topographic feedbacks[43]. The model shows these influence the 100-kyr eccentricity response primarily in North and East Africa. The North African feedback is identified in Armstrong, et al. [34] and discussed above. In East Africa, precipitation is sensitive to ice-sheet forcing of the IWC. During high (low) eccentricity interglacials (glacials), ice-sheet feedbacks result in comparatively warmer (cooler) East Indian Ocean SST anomalies (Supplementary Fig. 16), strengthening (weakening) the IWC (Supplementary Fig. 10), increasing (decreasing) convergence and decreasing (increasing) regional convective rainfall.

Imprinted on these mechanisms is eccentricity's modulation of precession. Due to the dominance of precession, this is the primary impact of eccentricity on African precipitation variability and occurs synchronously across the continent.

Obliquity

Our sensitivity analyses show that obliquity anomalies are driven by its impact on insolation (Supplementary Fig. 7i) and are not influenced by high latitude processes as has been previously proposed[21,22,44]. At high (low) obliquity, enhanced (reduced) summer insolation and seasonality shift the Hadley Cell, rainbelt and the ITCZ poleward (equatorward) (Supplementary Figs. 17 and 18). This strengthens (weakens) the summer convective systems that dominate the subequatorial regions. This is comparable to the precession forcing mechanism, although summer enhancement occurs in phase in both hemispheres. In Central Africa, this results in a poleward (equatorward) shift in the westerlies which reduces (increases) precipitation (Supplementary Fig. 17).

Because precession dominates the subequatorial regions, high (low) obliquity primarily increases (decreases) the amplitude of precession forcing (Supplementary Fig. 19). Thus, the precipitation response to obliquity depends on the precession phase, whereas the precession response is largely independent of obliquity. Modelled obliquity therefore acts as a second order control (after eccentricity) on the amplitude of precession forcing.

In the model the southern half of SE Africa shows decreased (increased) precipitation at high (low) obliquity. As discussed, regional precipitation is influenced by Agulhas Current SSTs. At high (low) obliquity, the enhanced (reduced) inter-hemispheric temperature gradient shifts the STF equatorward (poleward), resulting in a colder (warmer) Agulhas Current (Supplementary Fig. 14) and weaker (stronger) austral winter (JJA) South Indian Ocean southeasterlies (Supplementary Fig. 17), reducing (increasing) precipitation.

Discussion

The proxies and climate model dataset analysed in this study indicate that African hydroclimate variability over the mid-late Quaternary has been strongly coupled to orbital forcing. There is broad proxy-model consensus that eccentricity modulated precession is the dominant forcing, with increased rainfall in northern (southern) Hemisphere Africa at precession minima (maxima). The model demonstrates that eccentricity also impacts moisture via feedbacks associated with total insolation change, ice-sheet extent, and greenhouse gas concentrations. These act to enhance rainfall in approximate northern (southern) Hemisphere Africa at high (low) eccentricity, however, there remains uncertainty with proxies in East, Southwest and Southeast Africa, exacerbated by temporal limitations of records. Despite Africa's low latitude, the model and most proxies demonstrate obliquity forcing. High (low) obliquity is associated with enhanced subequatorial (equatorial) rainfall, although there is some discrepancy amongst proxies in West, Central and East Africa.

Recent studies[24] concluded that the dominant mode of orbital forcing over the past 620kyrs was an east-west antiphase associated with 400kyr-eccentricity due to its influence on the IWC. Our model indicates that 400kyr-eccentricity results in a Southwest-Northeast antiphase, however this is due to variability in the position of the seasonal rainbelt and is not linked to IWC feedbacks. However, the key role of 400kyr-eccentricity is to modulate precession forcing. Problematically, temporal limitations in proxies make it difficult to verify these conclusions.

Other studies have observed potential drying trends in Northeast[45], West[44] and East Africa[13,46], and wetter conditions in Lake Malawi[33]. However, we do not observe a long-term trend in modelled precipitation, or in our pollen reconstructions, in any region over the past 800kyr (Fig. 3c-h), consistent with Blumenthal, et al. [47] and Potts, et al. [48]. Castañeda, et al. [49] concluded that Southeast African variability accelerated following the Mid-Brunhes Transition (MBT; ~430 kyr BP). Whereas in East Africa, Lupien, et al. [46] demonstrated enhanced variability at both the MPT (~ 800kyr BP) and MBT, which they linked to high latitude feedbacks. Our model also shows enhanced variability at these time periods; however, this was driven by 400kyr and 100kyr eccentricity modulation of precession and was consistent pre and post MBT.

In order to address proxy-model consensus and outstanding uncertainty, we now consider the model and proxy evidence regionally (Methods) amongst the wider literature. Regional modelled precipitation timeseries are shown in Fig. 3c-h.

North Africa

The North African hydroclimate is highly sensitive to orbital forcing over the past 800kyrs. The observations (Sah1, Sah2, Horn, NE.Afr) and model indicate that this region is dominated by the precession minima paced NAHPs, which have been identified in numerous proxy and modelling studies[12,25,26,30,50–54] extending eastward to the Kenyan Rift Valley[55,56]. The influence of precession on

tropical monsoons, and its generation of a North-South African interhemispheric antiphase has therefore been well established[22,25,27,28,34,44,57,58].

Modelled precession amplitude is modulated by eccentricity and obliquity. Eccentricity also indirectly influences the NAHPs via its influence on the ice-sheets[34]. There is evidence for this from proxies[25,26,59,60] and sapropels[28,61,62]. However, although obliquity modulation has been identified in models[63,64], it is not explicit in the proxies. The precession forcing in North Africa is of greater magnitude to Southern Africa, consistent with the concept that Northern Hemisphere monsoons are more sensitive to precession than southern monsoons[65]. The proxies indicate a positive relationship with 400-kyr eccentricity (although not 75% confident), in agreement with the model.

Model and observations indicate that glacials (interglacials) were drier (wetter) and less (more) variable. This is consistent with numerous other proxy and modelling studies[22,53,54,66–69].

West Africa

The model demonstrates a regional dipole between the West (i.e. Liberia, Cote d'Ivoire and Ghana) and the East of the region. This may complicate proxy signals and interpretation. This antiphase is consistent with other glacial-interglacial modelling studies[68,69], and is therefore a robust feature in models.

The model indicates dominant eccentricity modulated precession forcing, however the observations (BOS, W.Afr) indicate dominant eccentricity and obliquity. This is consistent with studies offshore Liberia[21,22], which similarly demonstrated dominant eccentricity and obliquity and weaker precession forcing. DeMenocal, et al. [21] also show a negative 400kyr-eccentricity relationship, consistent with BOS, W.Afr and the model. However, Skonieczny, et al. [59] concluded that the prevalence of high latitude forcing in these studies is an artefact of their methods and precession is dominant. Additional proxies from this region are sparse and further observations are required to clarify regional sensitivity to orbital cyclicity.

The observations indicate wetter interglacials and drier glacials, as also shown in other modelling[67] and proxy studies[70,71].

Central Africa

The model indicates that Central Africa is the least sensitive region to orbital forcing due to its linear seasonal response to precession, resulting in a relatively stable hydroclimate. However, both observations show a considerate precession contribution (56% and 19%) to variability, in agreement with Zabel, et al. [72]. Obliquity is dominant in the model, however there are conflicting observation signals to corroborate the sign of its influence. Proxies may be influenced by their vast Congo River source and uncertainty regarding transport pathways, causing this proxy and proxy-model disparity. Problematically, additional long proxies from this region are sparse, and further studies are required to resolve

uncertainty. A study from a similar latitude in Eastern Brazil indicates dominant obliquity with moisture enhanced at low phases, lending support to our results[73]. It is intriguing that obliquity forcing is strong in this equatorial region despite its maximal high latitude impact.

The model and proxies agree that interglacials were wetter and glacials drier. This is consistent with other modelling[67,68] and proxy studies[74–78].

East Africa

The model indicates this region is sensitive to precession and ice-sheet forcing of the IWC. Model and observations (Mal1, Mal2, Koora) indicated enhanced precipitation at precession maxima. This is supported by additional Lake Malawi studies[79,80]. However there remains uncertainty regarding the position of the hinge line separating the precession hemispheres. In our model it extends to 4°S, bounding the region with a predominant Indian Ocean moisture source. However, studies from Lake Tanganyika[81] and Challa[82] indicate enhanced precession minima precipitation. This indicates our modelled hinge zone may be located too far North.

Similarly, there are conflicting proxy-model results regarding glacial-interglacial variability. The model indicates wetter (drier) glacials (interglacials), in disagreement with Mal2 and Koora. However, a regional summary of LGM proxies similarly indicates a wetter LGM[83,84], in agreement with our model. Nevertheless, there remains significant uncertainty amongst LGM moisture proxies, even within the same and proximal locations. Contrary to our model, additional studies from Lake Malawi[79,85,86] and pollen proxies from Lake Victoria[87], Challa[88–90], Tanganyika[81] and Rukwa[91] indicate a drier LGM. In contrast, a different Lake Challa proxy demonstrates a wetter LGM[82], consistent with proxies from Lake Masoko[92,93], Central Tanzania[94] and Kenya[95]. Proxy disparity may be exacerbated by the sensitivity of pollen records to low glacial atmospheric CO_2 concentrations[96,97], and lake level proxies (e.g. Mal2) may be influenced by regional tectonic activity which alters local basin geometry[46] which may complicate comparison[89]. A wetter LGM is consistent with some model studies[98], however a PMIP4 comparison shows a mixed response, with the ensemble mean showing little glacial-interglacial trend[69].

Precession and eccentricity forcing influence regional precipitation via their impact on Indian Ocean SSTs, the IWC and IOD. However there similarly remains significant model-proxy uncertainty regarding the response of the IWC to altered climate states[99], including glacial and interglacial variability[36,84,100–102], mid-Holocene forcing[100,103–109], and future anthropogenic warming[110–114]. A model intercomparison showed that HadCM3 is the only model to show significant IWC weakening during the LGM[36,101], which drives wetter glacial conditions. Here we show that this is due to ice-sheet forcing, which may exacerbate inter-model disparity due to the significant uncertainty regarding ice-sheet extent and elevation[115]. The modelled weaker LGM IWC and positive IOD is consistent with salinity and SST proxies from the Arabian Sea and the Indo-Pacific warm pool[83,101]. However, proxies for thermocline depth[116], Mozambique Channel throughflow[102], and other modelling studies[117] indicate a stronger glacial IWC.

Currently therefore the regional hydroclimate response to orbital forcing remains unclear. Potentially this region is highly spatio-heterogenous and tectonically sensitive which biases key lake sources. This is not captured in models and complicates proxy interpretation, highlighting an area of future work.

Southeast Africa

Modelled orbital forcing is antiphased between the southern half of SE Africa and northward of ~ 25°S. The Limpopo River basin falls in-between these zones, potentially causing the mixed signal in different proxies.

In the model the southern half of SE Africa is influenced by the Agulhas Current. The link between Southeast African rainfall and the Agulhas Current on orbital timescale has been previously identified[49,118]. Modelled and observed Agulhas Current SSTs[119] show good agreement, with variability dominated by obliquity and eccentricity (Supplementary Fig. 14b-c). In the model this region experiences wetter (drier) interglacials (glacials), which is also suggested by regional vegetation[49,118] and Plio-Pleistocene leaf wax δD records from Limpopo catchment[120]. However, the potential Limpopo basin dichotomy may influence transport pathways and therefore the proxies. This may be why there are inconsistencies in the proxy interglacial-glacial anomalies, as Lim1 and Lim2 may represent different areas of the basin. Furthermore, this antiphase is not shown in a CMIP5 ensemble[69], and is exhibited in only two other coupled models (MRI and IPSL)[121]. Similarly, Simon, et al. [29] showed only weak glacial-interglacial variability in the southern part of SE Africa. This result is therefore not robust across observations and models, possibly due to inaccurate sensitivity to the Agulhas Current, and further research is required to clarify its role and regional influence.

The proxies (Lim1, Lim2) and model show enhanced precession maxima precipitation. This is consistent with other studies[27,29,122], but in contrast to Chevalier and Chase [123].

In the North of the region the model indicates wetter glacials, in agreement with Zambezi River records[124,125] and models[69]. Chevalier and Chase [123] concluded that these wetter glacials were limited to ~ 15–20°S, however in our model they extend to ~ 25°S. Again, this may be due to modelled bias in the regional sensitivity to the Agulhas Current, which may have extended further North and West to the Cape observation. This may explain the inconsistencies between that observation and the modelled obliquity and eccentricity response in the Cape region.

Southwest Africa

Modelled variability is dominated by eccentricity modulated precession and 100kyr-eccentricity. The model and observations (Nam1, Nam2, Cape) indicate enhanced precession maxima precipitation. This has also been identified in pollen records[126,127] and speleothems[128]. However, Namib desert proxies[129] and lake level records from Botswana[130–132] indicate enhanced Holocene (precession minima) precipitation. Interestingly, Nam2 also indicates increased Holocene precipitation (Supplementary Fig. 1h) in contrast to earlier precession minima phases, signifying that this region may have responded

differently during the Holocene. Alternatively, the precession hinge line was located further south in Botswana, or lake level records were influenced by increased precession minima rainfall occurring further north in their source areas. Both model and observations indicate weak obliquity forcing, in contrast to a strong obliquity signal identified offshore Namibia by Daniau, et al. [133].

The model indicates more arid (humid) interglacials (glacials), in agreement with Nam1 and Nam2. This is consistent with studies evaluating the wider Southern Hemisphere subtropics[134], sediment records offshore Namibia[127,135–137], terrestrial records[129,138–140], and models[69,121]. However, there is disagreement with the Cape record, which may be due to this area's sensitivity to the Agulhas Current which is not captured in the model.

Implications for Hominin Evolution

The model and observations indicate that African hydroclimate variability is dominated by precession. High-resolution Plio-Pleistocene proxy records suggest that precessional variability has formed an important climatic context for early human evolution[55,141]. Sedimentary $\delta^{13}C$ data from Oldupai Gorge show recurrent vegetation changes following precessional cycles, where open grasslands turned into forest and vice versa in less than 10kyr[141]. Such rapid and profound ecosystem changes imply that animals, including humans, responded by adjusting their ranges to track their preferred habitats or by developing adaptations to cope with these changes in place, as is suggested by variability selection hypothesis[48,142]. In regions such as Lake Turkana and Oldupai Gorge, our modelled average precipitation over the past 800kyr is 235mm/yr and 670mm/yr, with precession maxima (minima) phases driving a contrasting peak precipitation change of -30% (+ 15%) and + 33% (-49%) respectively. Therefore, during extreme precession maxima phases Lake Turkana would have become unsuitable for human habitation, whereas Oldupai Gorge (700km south) could have supported expansion of tall grassland and woodland ecosystems, which would have changed to semi-arid grassland during extreme precession minima phases.

However, if humans had evolved mechanisms to cope with recurrent environmental changes related to precession variability, it is possible that the associated population density and distribution responses were not very strong during the Mid and Late Pleistocene. Furthermore, populations of human hunter-gatherers respond exponentially not linearly to changes in net primary productivity[143], which is controlled by African precipitation. Therefore, it is possible that the effects of precession only truly occurred during the phases of eccentricity amplified precessional variability.

It has been recently suggested that the evolution of *Homo sapiens* took place in an African-wide network of regional populations[144,145]. In this kind of continental meta-population, the strength of connections and the flow of genetic and cultural information between sub-population was controlled by climate variably affecting suitability of different regions. Our results demonstrate regional differences in climate trajectories that could potentially have driven human population dynamics postulated by the continental metapopulation model (Fig. 3). For example, North and West Africa broadly respond together, i.e.

enhanced rainfall at precession minima, with wetter (drier) more (less) variable interglacials (glacials). As Fig. 3 shows, this is in direct contrast to East Africa, which experiences enhanced rainfall at precession maxima, with drier (wetter) more (less) variable interglacials (glacials). This means that when the Sahara experienced humid phases and North African populations were connected to Sub-Saharan western and central Africa, East Africa was arid and less suitable. Regional contrasts can also be observed in southern Africa, where the southern half of SE Africa exhibits arid (humid) glacials (interglacials), while much of Austral subequatorial Africa shows an opposite pattern (Fig. 3). All these differences could have resulted in a complex spatio-temporal pattern of population growth and migration, where different regions acted as hubs of population growth and expansion at different phases of orbital cycles.

However, due to relatively stability of precipitation in Central Africa, and consistent high precipitation in West Africa, these regions may have provided continuous refuge and fostered relatively stable source populations over the past 800kyrs. These regions have not traditionally featured very prominently in archaeological and palaeoanthropological research, but recently it has become evident that this large region contains rich and numerous archaeological records[146]. From a purely climatic perspective this region could have produced surplus populations to feed more unstable regions in the north, east and south when they became suitable during different orbital phases.

While our results show 400kyr eccentricity-related SW-NE differences in precipitation, the pattern does not appear to be as strong and thus its impacts on human evolution as significant as has recently been suggested[23,24]. However, because of the above-mentioned non-linear effect of net primary productivity (precipitation) on human populations, even small geographical differences in the eccentricity amplification of precession can create long-term human population dynamics that are not readily visible just by looking at the climate patterns alone. Therefore, to make better sense of the impacts of the climate patterns observed in our model and proxy records on human population dynamics, we need to explicitly model those dynamics.

Methods

Proxies

In this study we analyse 17 moisture proxies from across Africa. Five (WAfr, Nam2, Cape, Lim2, Mal1) are new, quantitative reconstructions of mean annual precipitation (MAP) from fossil pollen sequences, generated using an ensemble of pollen-MAP calibration models as discussed below. We also use a pollen-based woody cover reconstruction from the Ghanian Lake Bosumtwi (BOS[147]), two Saharan Dust proxies from Atlantic marine cores offshore Sahara (Sah1[59], Sah2[25]), mineralogical and geochemical reconstructions downstream of the Congo River (Con1[148], Con2[149]), Limpopo River (Lim1[11]) and the Ethiopian Chew Bahir basin (CBH[6]), δD and $\delta^{13}C$ leaf wax reconstructions offshore Namibia (Nam1[150]),

the Kenyan Koora Basin (Koora[46]) and the Horn of Africa (Horn[60]), a Lake Malawi lake-level reconstruction (Mal2[33]), and an East Mediterranean geochemical derived humidity index (NE.Afr[26]).

Pollen Reconstructions

Fossil pollen records and chronological control

We have generated five new pollen-based quantitative reconstructions for this study, developed using five fossil pollen sites from Africa: MD96-2048 (Limpopo River mouth; 26º10'S, 34º01'E)[118,151]; Malawi Lake records, including MAL05-1B (11º18'S, 34º26'E)[152,153], MAL05-1C (11º18'S, 34º26'E)[152–154], M86-18P (11º19'S, 34º39'E) and M86-22P (13º01'S, 34º31'E)[155,156] ; GIK 16856-2 (4º48'N, 3º24'E)[157]; GeoB1711-4 (23º19'S, 12º22'E)[158]; IODP Site U1479 (35º03'S, 17º24'E)[126].

The chronologies of MD96-2048 (Limpopo), MAL05-1B and MAL05-1C (Malawi), GIK 16856-2 and IODP Site U1479 pollen records are based on the age-depth models from the original studies. The age control of M86-18P and M86-22P (Malawi), and GeoB1711-4 are based on the updated chronologies from Phelps, et al. [159]. The pollen data from each record and their corresponding chronological controls can be found in the Data availability section.

Pollen-based quantitative climate reconstruction technique

We prepared quantitative MAP reconstructions using an ensemble of six pollen–MAP calibration models, built on a set of modern (surface sediment) pollen samples from Africa combined with modern climate data. The calibration ensemble includes three classical approaches which are based on unimodal taxon response models and are commonly used to calibrate microfossil proxies, namely, the weighted averaging (WA)[160], weighted averaging-partial least squares (WA-PLS)[161], and maximum likelihood regression curves (MLRC)[160]. Also used were the modern analogue technique (MAT)[162] as well as two machine-learning methods based on ensemble models of regression trees, the random forest (RF)[163] and the boosted regression tree (BRT)[164]. The calibration models were implemented using the libraries *gbm*[165], *randomForest*[166], and *rioja*[167] for the R statistical software[168]. Finally, we synthesised the ensemble as the median curve of the six individual reconstructions. The 95% error margins of the median curve were estimated by calculating the median curve 1000 times from bootstrap samples of the six reconstructions and by extracting the 2.5th and 97.5th percentiles. In ten repeats of ten-fold cross-validation using the modern data, the calibration models show coefficients of determination ranging from 0.60 to 0.74 (Supplementary Fig. 20).

Modern pollen calibration set and climate data

We developed an African modern pollen dataset using 1571 surface-sediment pollen samples originating from the African Modern Pollen Database (AMPD[169–172]; Supplementary Fig. 21). The African fossil and modern pollen taxonomy was harmonised to 330 taxa, largely to either family or genus level. As a guideline, our harmonised data splits families to the constituent genera if such a split was done in most

of the individual pollen samples, thus allowing the distinct climatic response of each genus to be modelled in the MAP calibration models. The taxonomic level of pollen harmonization is broadly comparable with the European and North American modern pollen datasets commonly harmonized to ca. 60–70 pollen types, however the much larger diversity of woody plants in Africa results in a considerably larger number of pollen types. To remove the local climate signals and to more accurately reconstruct regional climate, aquatic plants were removed. The recent mean annual precipitation values for the modern pollen sites were extracted from the WorldClim v2.1 raster[173] with a 30-second resolution (https://worldclim.org/).

Modelled Climatology

HadCM3BB-v1.0 coupled climate model

We utilise an 800kyr climate model dataset generated utilising the HadCM3BB-v1.0 coupled climate model[34,37,38,174]. This is a variant of the HadCM3B climate model which is described in detailed in Valdes, et al. [38]. The model consists of an atmospheric component with a resolution of 2.5°x3.75°, 19 vertical levels, and a 30-minute timestep[175], and an ocean model with a resolution of 1.25°x1.25°, 20 vertical levels and a 1 hour timestep[176]. The levels are finer towards the Earth surface.

The model utilises version 2.1 of the Met Office Surface Exchange Scheme (MOSES)[177], which simulates the movement of water and energy, and the physiological processes of photosynthesis, transpiration, and respiration, which are regulated by stomatal conductance and consequently CO_2 concentration. MOSES 2.1 incorporates the fractional coverage of nine distinct surface types simulated by the dynamic global vegetation model (DGVM) TRIFFID. These include five plant functional types (PFTs); deciduous and needleleaf trees, C3 and C4 grasses, and shrubs, with the residual assigned to bare soil. Throughout the model simulation, the vegetation dynamically evolves based on temperature, moisture, CO_2 levels, and competition with other PFTs. The model does not incorporate an interactive ice model or carbon/methane cycle. These boundary conditions have been imposed as discussed below.

The update to the HadCM3B model follows work of Hopcroft, et al. [37]. It involved modifying the vertical profile of convective entrainment and detrainment and altering the moisture stress function of vegetation. This was shown to more accurately simulate the impact of precession on the West African Monsoon system, which subsequently improves the simulation of the North African Humid Periods[34,37]. The model has therefore been shown to more accurately simulate mid-Holocene precipitation in North Africa (and other regions) when compared to the majority of CMIP6 models (see Supplementary Fig. 1 of Armstrong, et al. [34]). In addition, the model is highly computationally efficient, which allows us to perform large ensemble studies.

A validation of HadCM3BB-v1.0 modelled precipitation, sea surface temperatures and surface air temperatures against a range of proxy observations is provided in the Supplementary Information in

Armstrong, et al. [34]. This demonstrates that the model accurately reproduces present day and long-term patterns in global climate.

Boundary Conditions

The boundary condition timeseries are shown in Supplementary Figure. The simulations are forced with orbital parameters from Berger, et al. [178] which are very well constrained. We utilise Greenhouse gas concentrations (CO_2, N_2O and CH_4) derived from the Vostok Ice core[179,180] which cover the period 0-800kyr BP.

The elevation and extent of the Fennoscandian, North American, Greenland, and Antarctic ice-sheets has been applied using the model reconstruction of de Boer, et al. [181]. This gives ice thickness and extent, which are used to calculate the continental elevation (depending on isostatic rebound and ice thickness), bathymetry, and the land-sea mask. There are significant uncertainties associated with ice-sheet reconstruction beyond the last glacial maximum (LGM), in part due to poor preservation following the last deglaciation. Although the ice area is approximated based on sea-level data, the structure of the ice-sheet during growth and decay phases remains uncertain which may impact the simulated climatology.

Experimental Set up

The boundary conditions have been utilised in 219 snapshot simulations spanning 0kyr BP (equivalent to the year 1950 but with pre-industrial greenhouse gas concentrations) to 800kyr BP. The simulations were performed at 1kyr intervals for 0-24kyr BP and 4kyr intervals for 24-800kyr BP. They have been run for 500 years which permits the surface ocean and atmosphere to reach a near equilibrium state, with analysis performed on the final 50 model years. This methodology permits the simulations to be run simultaneously and is therefore very efficient.

The snapshot climatologies are splined to a 100-yr timeseries for all variables utilised in the analysis. This has been performed using the ftcurv function of the NCAR command language (NCL)[182] which employs spline under tension. The data presented in this study is in native resolution and has not bias corrected.

Boundary condition sensitivity experiments

These simulations are analysed in the Supplementary Information. In order to identify how the different forcings associated with orbital variability (i.e. insolation, GHGs and ice-sheet variability) influence the African hydroclimate, we have performed two further sets of snapshot experiments (2x 219 simulations) using HadCM3BB-v1.0, each utilising the same set-up as described above.

The first set of simulations incorporates all forcings (as discussed) and is termed all_forcing. In order to identify the sole role of insolation change, we have re-run the simulations with just varying orbital parameters, utilising constant pre-industrial GHGs (CO2–280ppm, CH4–760ppbv, and N2O – 270ppbv) and ice-sheet extent and elevation. This is termed Orb_Only. In order to identify the role of greenhouse

gas forcing, we incorporate both orbital and GHG forcing with constant pre-industrial ice-sheets, termed Orb_GHG.

Precipitation vs P-E balance

Many of the proxies are representative of water availability, or precipitation-evaporation (P-E). Modelled P-E closely follows precipitation in each African region, with average correlation of 0.89 (Supplementary Fig. 4). In this study we focus specifically on annual precipitation (mm/day) variability, this Is consistent with the pollen based reconstructions of MAP and also permits us to avoid additional uncertainties associated with how modelled evaporation is parameterised[38].

Statistical Analysis

Spectral Analysis

Spectral analysis is performed using Fast Fourier Transform with the NCL function specx_anal. For each observation spectra, we isolated frequency bands which correspond to key orbital periodicities for 400kyr (380–420 kyr) and 100kyr eccentricity (90–120 kyr), obliquity (35–45 kyr) and precession (18–27 kyr). Confidence intervals are calculated using the spec_ci function, with a 75% confidence interval calculated compared to a stochastic (Markov) process. Where the average power in each orbital frequency band exceeds this confidence interval the orbital cycle is deemed to demonstrate a confident variability signal and is included in Fig. 1d-g.

Singular Spectrum Analysis (SSA)

Singular spectrum analysis is a statistical technique used to decompose a time-series into a range of periodicities and noise in order to extract a signal of interest. Here we use it to extricate specific orbital frequencies from the observations and model data. SSA has been used in a number of climatological studies investigating the dynamical nature of climate variability[183–186]. In this study we have performed SSA using the R-package Rssa, a detailed mathematical overview of SSA and its application to climate data, and an overview of the Rssa package including examples and code, is provided in Golyandina and Korobeynikov [40] and Golyandina, et al. [41].

For the observations, they are first interpolated to a consistent 100-year timescale using the NCL function linint1[182]. We log transformed the dataset of CBH to remove outliers so the data demonstrates an approximate normal distribution consistent with the other datasets. The interpolated observations are decomposed using the Rssa ‘ssa’ function into a set of eigenvalues and eigenvectors, following the methodology outlined in Section 4 of Golyandina and Korobeynikov [40]. We first define a window length (M) which is proportional to the potential periodic nature of the data as stated by Ghil [184]. The value of M for each observation depends on the statistical confidence of the orbital signals defined in the spectral analysis. For observations that demonstrate eccentricity, obliquity and precession variability at 75% confidence (BOS, Lim 2, Mal 2, CBH) we use an L value equivalent to 120kyrs. For those that

demonstrate confident obliquity and precession signals (Sah2, W.Afr, Con1, Con2, Nam1, Nam2, Cape, Koora, Horn, NE.Afr) we use an L value equivalent to 40kyrs, and for those that demonstrate only confident precession signals (Sah1, Lim1, Mal1) we use an L value equivalent to 20kyrs.

There are two stages of decomposition, the first to identify the slowly varying trend component, and the second to distinguish the variability component. Following the first decomposition, the trend is reconstructed and removed and the timeseries decomposed for a second time in order to identify the variability components of the timeseries. The original and detrended observations are shown in Supplementary Figs. 1 and 2 respectively.

The resultant components are then grouped depending on their frequencies using the Rssa 'grouping.auto' function. This function splits the timeseries variability components into groups using their frequencies that are measured by a periodogram. Frequencies are grouped around the key orbital periodicities for 400kyr (380–420 kyr) and 100kyr eccentricity (90–120 kyr), obliquity (35–45 kyr) and precession (18–27 kyr). The grouped components are combined, extracted, and reconstructed for each orbital frequency that is present. Note that combining all the reconstructed components, including the trend, would replicate the initial timeseries. Similarly, the sum of the variances of each of the reconstructed components is equal to the variance of the initial timeseries. We therefore calculate the variance of the reconstructed orbital components and show this as a proportion compared to the variance of the initial de-trended timeseries (Fig. 1d-g). This demonstrates how much each orbital frequency contributes to the overall variability within the de-trended timeseries. The reconstructed components with frequencies corresponding to orbital cycles are shown in Supplementary Fig. 2 with the de-trended observation timeseries. Only those frequencies that are deemed to be significant in the original timeseries (as discussed above) are shown.

For the model data, SSA analysis and grouping is carried out in the same way for the 800 kyr precipitation timeseries from each terrestrial grid box. The variance is calculated for each orbital cycle from the extracted and reconstructed signal, and the relative proportion of variance calculated against the total variance of the initial de-trended precipitation timeseries. These are shown in the filled contour map plots in Fig. 1d-g.

Next, we identify the anomalies during high-low / maximum-minimum orbital phases (Fig. 1h-k). The timeseries of the orbital cycles are shown in Supplementary Fig. 3, where periods of high and low eccentricity and obliquity, and maximum and minimum precession are shown as red and blue phases respectively. Orbital anomalies are calculated as the difference between the composite averages during periods of high-low/maximum-minimum/red-blue phases. For the observations, the crossed opaque circles show the anomalies of orbital cycles that are not deemed to be 75% confident (as defined above), which are calculated directly from the proxy timeseries. The bold colour circles represent 75% confident signals and are calculated from the extracted and reconstructed orbital timeseries components shown in Supplementary Fig. 2. Similarly, the modelled orbital anomalies are calculated by calculating the

precipitation difference during periods of high-low/maximum-minimum/red-blue orbital phases of the reconstructed orbital timeseries from each grid-box.

Defining African Climate Regions

In order to systematically assess observed and modelled orbital influence on African climate we split Africa into 6 regions as shown in Fig. 1a. These are characterised by different contemporary climate regimes based on the Köppen classification[187], their varied precipitation source region, and their different response to orbital forcing as demonstrated by the spatial patterns shown by the SSA orbital forcing analysis (Figs. 1 and 2). These regions are summarised as follows.

North Africa is characterised by a large meridional precipitation gradient, varying from the humid tropics dominated by the African rain belt and WAM, to the semi-arid Sahel and vast hyper-arid Sahara. Tropical West Africa sits beneath the boreal winter ITCZ and summer rainbelt where convection drives the WAM. This fuels high summer rainfall sourced via the westerlies off the tropical Atlantic Ocean and Gulf of Guinea. Central Africa is dominated by the Congo Basin characterised by a hot and wet climate throughout the year. Regional precipitation is controlled by the convective rain belt, driven by low level westward moisture advection from the equatorial Atlantic Ocean[188,189]. The region is bordered to the East by the topography of the East African rift valley. North, West and Central African precipitation is sourced via westerly moisture transport from the equatorial Atlantic Ocean. East Africa is a complex climatological region which experiences an atypical semi-arid equatorial climate, in part due to the topography of the rift valley and the rain shadow it generates. Moisture is primarily sourced via the Northeasterly trade wind off the Indian Ocean and is strongly coupled to Indian Ocean SSTs[42]. We have split South Africa into East and West, which reflects their different primary moisture sources, the Indian and Atlantic Oceans respectively. Southwest Africa is characterised by an arid to semi-arid climate, with moisture sourced from the South Atlantic Westerlies and Indian Ocean southeasterlies. Finally, Southeast Africa is characterised by a temperate to sub-tropical climate, with moisture sourced via the Indian Ocean Southeasterlies. Each of these regions are assessed separately in Section 4.

Declarations

Data Availability

A total of 657 model simulations were performed for this study. The raw model output and an overview of all the simulations is available at https://www.paleo.bristol.ac.uk/ummodel/scripts/papers/Armstrong_et_al_2024.html. A document outlining how to access the NetCDF data files used in this study can be found at https://www.paleo.bristol.ac.uk/ummodel/scripts/papers/Using_BRIDGE_webpages.pdf. The relevant NetCDF file names for surface variables, full height atmosphere files, and ocean files are “[exptname]a.pdcl[month].nc”, “[exptname]a.pccl[month].nc” and “[exptname]a.pfcl[month].nc” respectively, where [exptname] and [month] need to be defined by the user. The specific experiment names for each snapshot simulation are shown in the table in the provided link, and the month refers

either to individual months ("jan", “feb”, “mar” etc.), seasons (“djf”, “mam”, “jja”, “son”), or the annual mean (“ann”).

The original repositories for each of the pollen records and associated chronologies used in this study can be downloaded from the following locations. MD96-2048 (Limpopo)[118,151]: https://doi.org/10.1594/PANGAEA.771285 and https://doi.org/10.1594/PANGAEA.897922. MAL05-1B (Malawi)[152,153]: Neotoma database (Dataset ID: 48635). MAL05-1C (Malawi) [152–154]: Neotoma database (Dataset ID: 46700). M86-18P and M86-22P (Malawi)[155,156]: https://doi.org/10.1594/PANGAEA.905309 (Databases: Phelps, et al. [159], Vincens, et al. [93])

and https://doi.org/10.1594/PANGAEA.870867 (Database: Goñi, et al. [190]). GIK 16856 – 2[157]: https://doi.org/10.1594/PANGAEA.776472. GeoB1711-4[158]: https://doi.org/10.1594/PANGAEA.905309 (Database: Phelps, et al. [159], Vincens, et al. [93]). IODP Site U1479[126]: https://doi.org/10.1594/PANGAEA.930614.

The remaining proxy observation timeseries shown in Fig. 1 and the Supplementary Figures are downloadable as an electronic supplementary from the associated cited articles as identified in Table 1.

Code Availability

All scripts used to analyse the data and produce the Figures have been written using the NCAR command language (NCL, Version 6.4.0) and are available from the Zenodo repository:

https://doi.org/10.5281/zenodo.12805780

Acknowledgements

This work was carried out using the computational facilities of the Advanced Computing Research Centre, University of Bristol—http://www.bris.ac.uk/acrc (Bluecrystal). E.A. and M.T. acknowledge funding from Kone Foundation (grant number 202006876) and J.S.S. from the Research Council of Finland (project 331426). We thank Basil Davis for additional modern pollen site data.

Competing Interests Statement

The authors declare no competing interests.

References

1. Chase BM (2021) Orbital forcing in southern Africa: Towards a conceptual model for predicting deep time environmental change from an incomplete proxy record. Q Sci Rev 265. https://doi.org/10.1016/j.quascirev.2021.107050

2. Kutzbach JE (1981) Monsoon Climate of the Early Holocene - Climate experiment with the Earths Orbital parameters for 9000 years ago. Science 214:59–61. https://doi.org/10.1126/science.214.4516.59
3. Lupien RL et al (2022) Orbital controls on eastern African hydroclimate in the Pleistocene. Sci Rep 12. https://doi.org/10.1038/s41598-022-06826-z
4. Nicholson SE (2017) Climate and climatic variability of rainfall over eastern Africa. Rev Geophys 55:590–635. https://doi.org/10.1002/2016rg000544
5. Timmermann A et al (2022) Climate effects on archaic human habitats and species successions. Nature 604:495–. https://doi.org/10.1038/s41586-022-04600-9
6. Foerster V et al (2022) Pleistocene climate variability in eastern Africa influenced hominin evolution. Nat Geosci 15:805–. https://doi.org/10.1038/s41561-022-01032-y
7. Maslin MA, Christensen B (2007) Tectonics, orbital forcing, global climate change, and human evolution in Africa: introduction to the African paleoclimate special volume. J Hum Evol 53:443–464. https://doi.org/10.1016/j.jhevol.2007.06.005
8. Maslin MA, Shultz S, Trauth MH (2015) A synthesis of the theories and concepts of early human evolution. Philosophical Trans Royal Soc B-Biological Sci 370. https://doi.org/10.1098/rstb.2014.0064
9. Timmermann A, Friedrich T (2016) Late Pleistocene climate drivers of early human migration. Nature 538:92–. https://doi.org/10.1038/nature19365
10. Trauth MH et al (2021) Northern Hemisphere Glaciation, African climate and human evolution. Q Sci Rev 268. https://doi.org/10.1016/j.quascirev.2021.107095
11. Caley T et al (2018) A two-million-year-long hydroclimatic context for hominin evolution in southeastern Africa. Nature 560:76–. https://doi.org/10.1038/s41586-018-0309-6
12. Larrasoaña JC, Roberts AP, Rohling EJ (2013) Dynamics of Green Sahara Periods and Their Role in Hominin Evolution. PLoS ONE 8. https://doi.org/10.1371/journal.pone.0076514
13. Owen RB et al (2018) Progressive aridification in East Africa over the last half million years and implications for human evolution. Proc Natl Acad Sci USA 115:11174–11179. https://doi.org/10.1073/pnas.1801357115
14. Hart NCG, Washington R, Maidment RI (2019) Deep Convection over Africa: Annual Cycle, ENSO, and Trends in the Hotspots. J Clim 32:8791–8811. https://doi.org/10.1175/jcli-d-19-0274.1
15. Lüdecke HJ, Muller-Plath G, Wallace MG, Lüning S (2021) Decadal and multidecadal natural variability of African rainfall. J Hydrology-Regional Stud 34. https://doi.org/10.1016/j.ejrh.2021.100795
16. Palmer PI et al (2023) Drivers and impacts of Eastern African rainfall variability. Nat Reviews Earth Environ 4:254–270. https://doi.org/10.1038/s43017-023-00397-x
17. Berger AM (1988) Theory and Climate. *Reviews of Geophysics* 26, 624–657 https://doi.org/10.1029/RG026i004p00624

18. Hays JD, Imbrie J, Shackleton NJ (1976) Variations in Earths Orbit - Pacemaker of the Ice ages. Science 194:1121–1132. https://doi.org/10.1126/science.194.4270.1121
19. Imbrie J (1982) Astrononomical theory of the Pleistocene Ice ages - A brief historical review. Icarus 50:408–422. https://doi.org/10.1016/0019-1035(82)90132-4
20. Milankovitch M (1930) in *Köppen Geigersches Handbuch der Klimatologie* (eds W. Köppen & R Geiger)
21. DeMenocal PB, Ruddiman WF, Pokras EM (1993) Influences of high-latitude and low-latitude processes on African terrestrial climate - Pleistocene eolian recrods from Equatorial Atlantic Ocean Drilling Programme site-663. Paleoceanography 8:209–242. https://doi.org/10.1029/93pa02688
22. Tiedemann R, Sarnthein M, Shackleton NJ (1994) Astronomic timescale for the Pliocene Atlantic Delta18O and dust flux records of Ocean Drilling Program Site-659. Paleoceanography 9:619–638. https://doi.org/10.1029/94pa00208
23. Gosling WD, Scerri EML, Kaboth-Bahr S (2022) The climate and vegetation backdrop to hominin evolution in Africa. Philosophical Trans Royal Soc B-Biological Sci 377. https://doi.org/10.1098/rstb.2020.0483
24. Kaboth-Bahr S et al (2021) Paleo-ENSO influence on African environments and early modern humans. Proc Natl Acad Sci USA 118. https://doi.org/10.1073/pnas.2018277118
25. Crocker AJ et al (2022) Astronomically controlled aridity in the Sahara since at least 11 million years ago. Nat Geosci 15:671–. https://doi.org/10.1038/s41561-022-00990-7
26. Grant KM et al (2017) A 3 million year index for North African humidity/aridity and the implication of potential pan-African Humid periods. Q Sci Rev 171:100–118. https://doi.org/10.1016/j.quascirev.2017.07.005
27. Partridge TC, Demenocal PB, Lorentz SA, Paiker MJ, Vogel JC (1997) Orbital forcing of climate over South Africa: A 200,000-year rainfall record from the Pretoria Saltpan. Q Sci Rev 16:1125–1133. https://doi.org/10.1016/s0277-3791(97)00005-x
28. Rossignol-Strick M (1985) Mediterranean Quaternary sapropels, an immediate response of the African Monsoon to variation in insolation. Palaeogeography Palaeoclimatology Palaeoecology 49:237–263. https://doi.org/10.1016/0031-0182(85)90056-2
29. Simon MH et al (2015) Eastern South African hydroclimate over the past 270,000 years. Sci Rep 5. https://doi.org/10.1038/srep18153
30. Tierney JE, Pausata FSR, deMenocal PB (2017) Rainfall regimes of the Green Sahara. Sci Adv 3. https://doi.org/10.1126/sciadv.1601503
31. Trauth MH et al (2007) High- and low-latitude forcing of Plio-Pleistocene East African climate and human evolution. J Hum Evol 53:475–486. https://doi.org/10.1016/j.jhevol.2006.12.009
32. Duesing W et al (2021) Changes in the cyclicity and variability of the eastern African paleoclimate over the last 620 kyrs. Q Sci Rev 273. https://doi.org/10.1016/j.quascirev.2021.107219

33. Johnson TC et al (2016) A progressively wetter climate in southern East Africa over the past 1.3 million years. Nature 537:220–. https://doi.org/10.1038/nature19065
34. Armstrong E, Tallavaara M, Hopcroft PO, Valdes PJ (2023) North African humid periods over the past 800,000 years. Nat Commun 14. https://doi.org/10.1038/s41467-023-41219-4
35. Brierley CM et al (2020) Large-scale features and evaluation of the PMIP4-CMIP6 < i > midHolocene simulations. Clim Past 16:1847–1872. https://doi.org/10.5194/cp-16-1847-2020
36. Harrison SP et al (2015) Evaluation of CMIP5 palaeo-simulations to improve climate projections. Nat Clim Change 5:735–743. https://doi.org/10.1038/nclimate2649
37. Hopcroft PO, Valdes PJ, Ingram W (2021) Using the Mid-Holocene Greening of the Sahara to Narrow Acceptable Ranges on Climate Model Parameters. Geophys Res Lett 48. https://doi.org/10.1029/2020gl092043
38. Valdes PJ et al (2017) The BRIDGE HadCM3 family of climate models: HadCM3@Bristol v1.0. Geosci Model Dev 10:3715–3743. https://doi.org/10.5194/gmd-10-3715-2017
39. Broomhead DS, King GP, EXTRACTING QUALITATIVE DYNAMICS, FROM EXPERIMENTAL-DATA (1986) Phys D 20:217–236. https://doi.org/10.1016/0167-2789(86)90031-x
40. Golyandina N, Korobeynikov A (2014) Basic Singular Spectrum Analysis and forecasting with R. Comput Stat Data Anal 71:934–954. https://doi.org/10.1016/j.csda.2013.04.009
41. Golyandina N, Korobeynikov A, Shlemov A, Usevich K (2015) Multivariate and 2D Extensions of Singular Spectrum Analysis with the Rssa Package. J Stat Softw 67:1–78
42. Tierney JE, Smerdon JE, Anchukaitis KJ, Seager R (2013) Multidecadal variability in East African hydroclimate controlled by the Indian Ocean. Nature 493:389–392. https://doi.org/10.1038/nature11785
43. Gao Y, Liu ZY, Lu ZY (2020) Dynamic Effect of Last Glacial Maximum Ice Sheet Topography on the East Asian Summer Monsoon. J Clim 33:6929–6944. https://doi.org/10.1175/jcli-d-19-0562.1
44. DeMenocal PB (1995) Plio-Pleistocene African Climate. Science 270:53–59. https://doi.org/10.1126/science.270.5233.53
45. Cerling TE et al (2011) Woody cover and hominin environments in the past 6 million years. Nature 476:51–56. https://doi.org/10.1038/nature10306
46. Lupien RL et al (2021) Eastern African environmental variation and its role in the evolution and cultural change of Homo over the last 1 million years. J Hum Evol 157. https://doi.org/10.1016/j.jhevol.2021.103028
47. Blumenthal SA et al (2017) Aridity and hominin environments. Proc Natl Acad Sci USA 114:7331–7336. https://doi.org/10.1073/pnas.1700597114
48. Potts R et al (2020) Increased ecological resource variability during a critical transition in hominin evolution. Sci Adv 6. https://doi.org/10.1126/sciadv.abc8975
49. Castañeda IS et al (2016) Middle to Late Pleistocene vegetation and climate change in subtropical southern East Africa. Earth Planet Sci Lett 450:306–316. https://doi.org/10.1016/j.epsl.2016.06.049

50. Ehrmann W, Schmiedl G, Seidel M, Krüger S, Schulz H (2016) A distal 140 kyr sediment record of Nile discharge and East African monsoon variability. Clim Past 12:713–727. https://doi.org/10.5194/cp-12-713-2016
51. Osborne AH et al (2008) A humid corridor across the Sahara for the migration of early modern humans out of Africa 120,000 years ago. Proc Natl Acad Sci USA 105:16444–16447. https://doi.org/10.1073/pnas.0804472105
52. Pausata FSR et al (2020) The Greening of the Sahara: Past Changes and Future Implications. One Earth 2:235–250. https://doi.org/10.1016/j.oneear.2020.03.002
53. Tjallingii R et al (2008) Coherent high- and low-latitude control of the northwest African hydrological balance. Nat Geosci 1:670–675. https://doi.org/10.1038/ngeo289
54. Wagner B et al (2019) Mediterranean winter rainfall in phase with African monsoons during the past 1.36 million years. Nature 573:256–. https://doi.org/10.1038/s41586-019-1529-0
55. Joordens JCA et al (2011) An astronomically-tuned climate framework for hominins in the Turkana Basin. Earth Planet Sci Lett 307:1–8. https://doi.org/10.1016/j.epsl.2011.05.005
56. Kingston JD, Deino AL, Edgar RK, Hill A (2007) Astronomically forced climate change in the Kenyan Rift Valley 2.7–2.55 Ma: implications for the evolution of early hominin ecosystems. J Hum Evol 53:487–503. https://doi.org/10.1016/j.jhevol.2006.12.007
57. Cheng H, Sinha A, Wang XF, Cruz FW, Edwards RL (2012) The Global Paleomonsoon as seen through speleothem records from Asia and the Americas. Clim Dyn 39:1045–1062. https://doi.org/10.1007/s00382-012-1363-7
58. Kutzbach JE, Liu XD, Liu ZY, Chen GS (2008) Simulation of the evolutionary response of global summer monsoons to orbital forcing over the past 280,000 years. Clim Dyn 30:567–579. https://doi.org/10.1007/s00382-007-0308-z
59. Skonieczny C et al (2019) Monsoon-driven Saharan dust variability over the past 240,000 years. Sci Adv 5. https://doi.org/10.1126/sciadv.aav1887
60. Tierney JE, deMenocal PB, Zander P (2017) D. A climatic context for the out-of-Africa migration. Geology 45:1023–1026. https://doi.org/10.1130/g39457.1
61. Emeis KC, Sakamoto T, Wehausen R, Brumsack HJ (2000) The sapropel record of the eastern Mediterranean Sea - results of Ocean Drilling Program Leg 160. Palaeogeography Palaeoclimatology Palaeoecology 158:371–395. https://doi.org/10.1016/s0031-0182(00)00059-6
62. Larrasoana JC (2021) A review of West African monsoon penetration during Green Sahara periods; implications for human evolution and dispersals over the last three million years. Oxf Open Clim Change 1. https://doi.org/https://doi.org/10.1093/oxfclm/kgab011
63. Bosmans JHC, Drijfhout SS, Tuenter E, Hilgen FJ, Lourens LJ (2015) Response of the North African summer monsoon to precession and obliquity forcings in the EC-Earth GCM. Clim Dyn 44:279–297. https://doi.org/10.1007/s00382-014-2260-z
64. Tuenter E, Weber SL, Hilgen FJ, Lourens LJ (2003) The response of the African summer monsoon to remote and local forcing due to precession and obliquity. Glob Planet Change 36:219–235.

https://doi.org/10.1016/s0921-8181(02)00196-0

65. Jalihal C, Bosmans JHC, Srinivasan J, Chakraborty A (2019) The response of tropical precipitation to Earth's precession: the role of energy fluxes and vertical stability. Clim Past 15:449–462. https://doi.org/10.5194/cp-15-449-2019
66. Kinsley CW et al (2022) Orbital- and Millennial-Scale Variability in Northwest African Dust Emissions Over the Past 67,000 years. Paleoceanography Paleoclimatology 37. https://doi.org/10.1029/2020pa004137
67. Nikolova I, Yin Q, Berger A, Singh UK, Karami MP (2013) The last interglacial (Eemian) climate simulated by LOVECLIM and CCSM3. Clim Past 9:1789–1806. https://doi.org/10.5194/cp-9-1789-2013
68. Pedersen RA, Langen PL, Vinther BM (2017) The last interglacial climate: comparing direct and indirect impacts of insolation changes. Clim Dyn 48:3391–3407. https://doi.org/10.1007/s00382-016-3274-5
69. Scussolini P et al (2019) Agreement between reconstructed and modeled boreal precipitation of the Last Interglacial. Sci Adv 5. https://doi.org/10.1126/sciadv.aax7047
70. Jahns S, Huls M, Sarnthein M (1998) Vegetation and climate history of west equatorial Africa based on a marine pollen record off Liberia (site GIK 16776) covering the last 400,000 years. Rev Palaeobot Palynol 102:277–288
71. Lézine AM, Izumi K, Kageyama M, Achoundong G (2019) A 90,000-year record of Afromontane forest responses to climate change. Science 363:177–181. https://doi.org/10.1126/science.aav6821
72. Zabel M et al (2001) Late Quaternary climate changes in central Africa as inferred from terrigenous input to the Niger fan. Quatern Res 56:207–217. https://doi.org/10.1006/qres.2001.2261
73. Hou A et al (2022) Obliquity Influence on Low-Latitude Coastal Precipitation in Eastern Brazil During the Past ∼850 kyr. Paleoceanography Paleoclimatology 37. https://doi.org/10.1029/2021pa004238
74. Anhuf D et al (2006) Paleo-environmental change in Amazonian and African rainforest during the LGM. Palaeogeography Palaeoclimatology Palaeoecology 239:510–527. https://doi.org/10.1016/j.palaeo.2006.01.017
75. Gasse F (2000) Hydrological changes in the African tropics since the Last Glacial Maximum. Q Sci Rev 19:189–211. https://doi.org/10.1016/s0277-3791(99)00061-x
76. Holtvoeth J, Wagner T, Horsfield B, Schubert CJ, Wand U (2001) Late-Quaternary supply of terrigenous organic matter to the Congo deep-sea fan (ODP site 1075): implications for equatorial African paleoclimate. Geo-Mar Lett 21:23–33
77. Maley J, Brenac P (1998) Vegetation dynamics, palaeoenvironments and climatic changes in the forests of western Cameroon during the last 28,000 years BP. Rev Palaeobot Palynol 99:157–187. https://doi.org/10.1016/s0034-6667(97)00047-x
78. Schefuss E, Schouten S, Schneider RR (2005) Climatic controls on central African hydrology during the past 20,000 years. Nature 437:1003–1006. https://doi.org/10.1038/nature03945

79. Castañeda IS, Werne JP, Johnson TC (2007) Wet and arid phases in the southeast African tropics since the Last Glacial Maximum. Geology 35:823–826. https://doi.org/10.1130/g23916a.1
80. Konecky BL et al (2011) Atmospheric circulation patterns during late Pleistocene climate changes at Lake Malawi, Africa. Earth Planet Sci Lett 312:318–326. https://doi.org/10.1016/j.epsl.2011.10.020
81. Tierney JE et al (2008) Northern hemisphere controls on tropical southeast African climate during the past 60,000 years. Science 322:252–255. https://doi.org/10.1126/science.1160485
82. Tierney JE, Russell JM, Damsté JSS, Huang YS, Verschuren D (2011) Late Quaternary behavior of the East African monsoon and the importance of the Congo Air Boundary. Q Sci Rev 30:798–807. https://doi.org/10.1016/j.quascirev.2011.01.017
83. DiNezio PN, Tierney JE (2013) The effect of sea level on glacial Indo-Pacific climate. Nat Geosci 6:485–491. https://doi.org/10.1038/ngeo1823
84. DiNezio PN et al (2018) Glacial changes in tropical climate amplified by the Indian Ocean. Sci Adv 4. https://doi.org/10.1126/sciadv.aat9658
85. Castañeda IS, Werne JP, Johnson TC, Filley TR (2009) Late Quaternary vegetation history of southeast Africa: The molecular isotopic record from Lake Malawi. Palaeogeography Palaeoclimatology Palaeoecology 275:100–112. https://doi.org/10.1016/j.palaeo.2009.02.008
86. Johnson TC et al (2002) A high-resolution paleoclimate record spanning the past 25,000 years in southern East Africa. Science 296:113–. https://doi.org/10.1126/science.1070057
87. Johnson TC et al (1996) Late pleistocene desiccation of Lake Victoria and rapid evolution of cichlid fishes. Science 273:1091–1093. https://doi.org/10.1126/science.273.5278.1091
88. Barker PA et al (2011) Seasonality in equatorial climate over the past 25 k.y. revealed by oxygen isotope records from Mount Kilimanjaro. Geology 39:1111–1114. https://doi.org/10.1130/g32419.1
89. Damsté JSS et al (2011) A 25,000-year record of climate-induced changes in lowland vegetation of eastern equatorial Africa revealed by the stable carbon-isotopic composition of fossil plant leaf waxes. Earth Planet Sci Lett 302:236–246. https://doi.org/10.1016/j.epsl.2010.12.025
90. Verschuren D et al (2009) Half-precessional dynamics of monsoon rainfall near the East African Equator. Nature 462:637–641. https://doi.org/10.1038/nature08520
91. Vincens A, Buchet G, Williamson D, Taieb M (2005) A 23,000 year pollen record from Lake Rukwa (8°S, SW Tanzania):: New data on vegetation dynamics and climate in Central Eastern Africa. Rev Palaeobot Palynol 137:147–162. https://doi.org/10.1016/j.revpalbo.2005.06.001
92. Garcin Y et al (2006) Centennial to millennial changes in maar-lake deposition during the last 45,000 years in tropical Southern Africa (Lake Masoko, Tanzania). Palaeogeography Palaeoclimatology Palaeoecology 239:334–354. https://doi.org/10.1016/j.palaeo.2006.02.002
93. Vincens A, Garcin Y, Buchet G (2007) Influence of rainfall seasonality on African lowland vegetation during the Late Quaternary: pollen evidence from Lake Masoko, Tanzania. J Biogeogr 34:1274–1288. https://doi.org/10.1111/j.1365-2699.2007.01698.x

94. Mumbi CT, Marchant R, Hooghiemstra H, Wooller MJ (2008) Late Quaternary vegetation reconstruction from the Eastern Arc Mountains, Tanzania. Quatern Res 69:326–341. https://doi.org/10.1016/j.yqres.2007.10.012
95. Perrott RA, Street-Perrott FA (1982) New evidence for a late Pleistocene wet phase in northern intertropical Africa. Palaeoecology Afr 14:57–76
96. Jolly D, Haxeltine A (1997) Effect of low glacial atmospheric CO2 on tropical African montane vegetation. Science 276:786–788. https://doi.org/10.1126/science.276.5313.786
97. StreetPerrott FA et al (1997) Impact of lower atmospheric carbon dioxide on tropical mountain ecosystems. Science 278:1422–1426. https://doi.org/10.1126/science.278.5342.1422
98. Kim SJ et al (2008) High-resolution climate simulation of the last glacial maximum. Clim Dyn 31:1–16. https://doi.org/10.1007/s00382-007-0332-z
99. Cai WJ et al (2013) Projected response of the Indian Ocean Dipole to greenhouse warming. Nat Geosci 6:999–1007. https://doi.org/10.1038/ngeo2009
100. Brierley C, Thirumalai K, Grindrod E, Barnsley J (2023) Indian Ocean variability changes in the Paleoclimate Modelling Intercomparison Project. Clim Past 19:681–701. https://doi.org/10.5194/cp-19-681-2023
101. Di Nezio PN et al (2016) The climate response of the Indo-Pacific warm pool to glacial sea level. Paleoceanography 31:866–894. https://doi.org/10.1002/2015pa002890
102. van der Lubbe HJL et al (2021) Indo-Pacific Walker circulation drove Pleistocene African aridification. Nature 598:618–. https://doi.org/10.1038/s41586-021-03896-3
103. Abram NJ et al (2020) Palaeoclimate perspectives on the Indian Ocean Dipole. Q Sci Rev 237. https://doi.org/10.1016/j.quascirev.2020.106302
104. Brown J, Lynch AH, Marshall AG (2009) Variability of the Indian Ocean Dipole in coupled model paleoclimate simulations. J Geophys Research-Atmospheres 114. https://doi.org/10.1029/2008jd010346
105. Cui K, Wang YB, Liu XQ, Shen J, Wang Y (2022) Holocene variation in the Indian Summer Monsoon modulated by the tropical Indian Ocean sea-surface temperature mode. CATENA 215. https://doi.org/10.1016/j.catena.2022.106302
106. Iwakiri T, Watanabe M (2019) Strengthening of the Indian Ocean Dipole With Increasing Seasonal Cycle in the Mid-Holocene. Geophys Res Lett 46:8320–8328. https://doi.org/10.1029/2019gl083088
107. Liu SS et al (2023) Weakening of the Indian Ocean Dipole in the Mid-Holocene due to the Mean Oceanic Climatology Change. J Clim 36:5363–5380. https://doi.org/10.1175/jcli-d-22-0878.1
108. Wang Y, Jian ZM, Zhao P, Chen JM, Xiao D (2015) Precessional forced evolution of the Indian Ocean Dipole. J Geophys Research-Oceans 120:3747–3760. https://doi.org/10.1002/2015jc010713
109. Weldeab S et al (2022) Impact of Indian Ocean surface temperature gradient reversals on the Indian Summer Monsoon. Earth Planet Sci Lett 578. https://doi.org/10.1016/j.epsl.2021.117327

110. England MH et al (2014) Recent intensification of wind-driven circulation in the Pacific and the ongoing warming hiatus. Nat Clim Change 4:222–227. https://doi.org/10.1038/nclimate2106
111. L'Heureux ML, Lee S, Lyon B (2013) Recent multidecadal strengthening of the Walker circulation across the tropical Pacific. Nat Clim Change 3:571–576. https://doi.org/10.1038/nclimate1840
112. Sharma S, Ha KJ, Cai WJ, Chung ES, Bódai T (2022) Local meridional circulation changes contribute to a projected slowdown of the Indian Ocean Walker circulation. Npj Clim Atmospheric Sci 5. https://doi.org/10.1038/s41612-022-00242-w
113. Tokinaga H, Xie SP, Deser C, Kosaka Y, Okumura YM (2012) Slowdown of the Walker circulation driven by tropical Indo-Pacific warming. Nature 491:439–443. https://doi.org/10.1038/nature11576
114. Vecchi GA, Soden BJ (2007) Global warming and the weakening of the tropical circulation. J Clim 20:4316–4340. https://doi.org/10.1175/jcli4258.1
115. Justino F, Timmermann A, Merkel U, Peltier WR (2006) An initial intercomparison of atmospheric and oceanic climatology for the ICE-5G and ICE-4G models of LGM paleotopography. J Clim 19:3–14. https://doi.org/10.1175/jcli3603.1
116. Mohtadi M, Prange M, Schefuss E, Jennerjahn TC (2017) Late Holocene slowdown of the Indian Ocean Walker circulation. Nat Commun 8. https://doi.org/10.1038/s41467-017-00855-3
117. Ma JL, Yan Q, Jiang NX, Wang HJ (2023) Antiphase change in Walker Circulation between the Pacific Ocean and the Indian Ocean during the Last Interglacial induced by interbasin sea surface temperature anomaly contrast. Clim Dyn. https://doi.org/10.1007/s00382-023-07039-4
118. Dupont LM et al (2011) Glacial-interglacial vegetation dynamics in South Eastern Africa coupled to sea surface temperature variations in the Western Indian Ocean. Clim Past 7:1209–1224. https://doi.org/10.5194/cp-7-1209-2011
119. Caley T et al (2011) High-latitude obliquity as a dominant forcing in the Agulhas current system. Clim Past 7:1285–1296. https://doi.org/10.5194/cp-7-1285-2011
120. Taylor AK et al (2021) Plio-Pleistocene Continental Hydroclimate and Indian Ocean Sea Surface Temperatures at the Southeast African Margin. Paleoceanography Paleoclimatology 36. https://doi.org/10.1029/2020pa004186
121. Engelbrecht FA et al (2019) Downscaling Last Glacial Maximum climate over southern Africa. Q Sci Rev 226. https://doi.org/10.1016/j.quascirev.2019.105879
122. Burns SJ et al (2022) Southern Hemisphere controls on ITCZ variability in southwest Madagascar over the past 117,000 years. Q Sci Rev 276. https://doi.org/10.1016/j.quascirev.2021.107317
123. Chevalier M, Chase BM (2015) Southeast African records reveal a coherent shift from high- to low-latitude forcing mechanisms along the east African margin across last glacial-interglacial transition. Q Sci Rev 125:117–130. https://doi.org/10.1016/j.quascirev.2015.07.009
124. Schefuss E, Kuhlmann H, Mollenhauer G, Prange M, Patzold J (2011) Forcing of wet phases in southeast Africa over the past 17,000 years. Nature 480:509–512. https://doi.org/10.1038/nature10685

125. Wang YV et al (2013) What does leaf wax δD from a mixed C3/C4 vegetation region tell us? Geochem Cosmochim Acta 111:128–139
126. Dupont LM, Zhao XQ, Charles C, Faith JT, Braun D (2022) Continuous vegetation record of the Greater Cape Floristic Region (South Africa) covering the past 300 000 years (IODP U1479). Clim Past 18:1–21. https://doi.org/10.5194/cp-18-1-2022
127. Urrego DH, Goñi MFS, Daniau AL, Lechevrel S, Hanquiez V (2015) Increased aridity in southwestern Africa during the warmest periods of the last interglacial. Clim Past 11:1417–1431. https://doi.org/10.5194/cp-11-1417-2015
128. Braun K et al (2019) Late Pleistocene records of speleothem stable isotopic compositions from Pinnacle Point on the South African south coast. Quatern Res 91:265–288. https://doi.org/10.1017/qua.2018.61
129. Chase BM et al (2019) Orbital controls on Namib Desert hydroclimate over the past 50,000 years. Geology 47:867–871. https://doi.org/10.1130/g46334.1
130. Burrough SL, Thomas DSG, Bailey RM (2009) Mega-Lake in the Kalahari: A Late Pleistocene record of the Palaeolake Makgadikgadi system. Q Sci Rev 28:1392–1411. https://doi.org/10.1016/j.quascirev.2009.02.007
131. Burrough SL, Thomas DSG, Shaw PA, Bailey RM (2007) Multiphase quaternary highstands at lake Ngami, Kalahari, northern Botswana. Palaeogeography Palaeoclimatology Palaeoecology 253:280–299. https://doi.org/10.1016/j.palaeo.2007.06.010
132. Cordova CE, Scott L, Chase BM, Chevalier M (2017) Late Pleistocene-Holocene vegetation and climate change in the Middle Kalahari, Lake Ngami, Botswana. Q Sci Rev 171:199–215. https://doi.org/10.1016/j.quascirev.2017.06.036
133. Daniau AL et al (2023) Precession and obliquity forcing of the South African monsoon revealed by sub-tropical fires. Q Sci Rev 310. https://doi.org/10.1016/j.quascirev.2023.108128
134. Weij R et al (2024) Elevated Southern Hemisphere moisture availability during glacial periods. Nature 626. https://doi.org/10.1038/s41586-023-06989-3
135. Pichevin L, Cremer M, Giraudeau J, Bertrand P (2005) A 190 ky record of lithogenic grain-size on the Namibian slope: Forging a tight link between past wind-strength and coastal upwelling dynamics. Mar Geol 218:81–96. https://doi.org/10.1016/j.margeo.2005.04.003
136. Stuut JBW, Lamy F (2004) Climate variability at the southern boundaries of the Namib (Southwestern Africa) and Atacama (northern Chile) coastal deserts during the last 120,000 year. Quatern Res 62:301–309. https://doi.org/10.1016/j.yqres.2004.08.001
137. Stuut JBW et al (2002) A 300-kyr record of aridity and wind strength in southwestern Africa: inferences from grain-size distributions of sediments on Walvis Ridge, SE Atlantic. Mar Geol 180:221–233. https://doi.org/10.1016/s0025-3227(01)00215-8
138. Chase BM, Meadows ME (2007) Late Quaternary dynamics of southern Africa's winter rainfall zone. Earth Sci Rev 84:103–138. https://doi.org/10.1016/j.earscirev.2007.06.002

139. Lim S, Chase BM, Chevalier M, Reimer PJ (2016) 50,000 years of vegetation and climate change in the southern Namib Desert, Pella, South Africa. Palaeogeography Palaeoclimatology Palaeoecology 451:197–209. https://doi.org/10.1016/j.palaeo.2016.03.001
140. Scott L, Marais E, Brook GA (2004) Fossil hyrax dung and evidence of Late Pleistocene and Holocene vegetation types in the Namib Desert. J Quat Sci 19:829–832. https://doi.org/10.1002/jqs.870
141. Magill CR, Ashley GM, Freeman KH (2013) Ecosystem variability and early human habitats in eastern Africa. Proc Natl Acad Sci USA 110:1167–1174. https://doi.org/10.1073/pnas.1206276110
142. Potts R, Faith JT (2015) Alternating high and low climate variability: The context of natural selection and speciation in Plio-Pleistocene hominin evolution. J Hum Evol 87:5–20. https://doi.org/10.1016/j.jhevol.2015.06.014
143. Tallavaara M, Eronen JT, Luoto M (2018) Productivity, biodiversity, and pathogens influence the global hunter-gatherer population density. Proc Natl Acad Sci USA 115:1232–1237. https://doi.org/10.1073/pnas.1715638115
144. Scerri EML, Chikhi L, Thomas MG (2019) Beyond multiregional and simple out-of-Africa models of human evolution. Nat Ecol Evol 3:1370–1372. https://doi.org/10.1038/s41559-019-0992-1
145. Scerri EML et al (2018) Did Our Species Evolve in Subdivided Populations across Africa, and Why Does It Matter? Trends Ecol Evol 33:582–594. https://doi.org/10.1016/j.tree.2018.05.005
146. Cerasoni JN et al (2022) Archaeological sites and palaeoenvironments of Pleistocene West Africa. J Maps 18:630–637. https://doi.org/10.1080/17445647.2022.2052767
147. Gosling WD et al (2022) A stronger role for long-term moisture change than for CO < sub > 2 in determining tropical woody vegetation change. Science 376:653–. https://doi.org/10.1126/science.abg4618
148. Schneider RR, Price B, Muller PJ, Kroon D, Alexander I (1997) Monsoon related variations in Zaire (Congo) sediment load and influence of fluvial silicate supply on marine productivity in the east equatorial Atlantic during the last 200,000 years. Paleoceanography 12:463–481. https://doi.org/10.1029/96pa03640
149. Gingele FX, Muller PM, Schneider RR (1998) Orbital forcing of freshwater input in the Zaire Fan area - clay mineral evidence from the last 200 kyr. Palaeogeography Palaeoclimatology Palaeoecology 138:17–26. https://doi.org/10.1016/s0031-0182(97)00121-1
150. Collins JA, Schefuss E, Govin A, Mulitza S, Tiedemann R (2014) Insolation and glacial-interglacial control on southwestern African hydroclimate over the past 140 000 years. Earth Planet Sci Lett 398:1–10. https://doi.org/10.1016/j.epsl.2014.04.034
151. Dupont LM, Caley T, Castañeda IS (2019) Effects of atmospheric CO2 variability of the past 800 kyr on the biomes of southeast Africa. Clim Past 15:1083–1097. https://doi.org/10.5194/cp-15-1083-2019
152. Ivory SJ et al (2016) Environmental change explains cichlid adaptive radiation at Lake Malawi over the past 1.2 million years. Proc Natl Acad Sci USA 113:11895–11900.

https://doi.org/10.1073/pnas.1611028113

153. Ivory SJ, Lézine AM, Vincens A, Cohen AS (2018) Waxing and waning of forests: Late Quaternary biogeography of southeast Africa. Glob Change Biol 24:2939–2951. https://doi.org/10.1111/gcb.14150
154. Beuning KRM, Zimmerman KA, Ivory SJ, Cohen AS (2011) Vegetation response to glacial-interglacial climate variability near Lake Malawi in the southern African tropics. Palaeogeography Palaeoclimatology Palaeoecology 303:81–92. https://doi.org/10.1016/j.palaeo.2010.01.025
155. DeBusk GH (1994) Transport and stratigraphy of pollen in Lake Malawi, Africa. Duke University
156. DeBusk GH (1998) A 37,500-year pollen record from Lake Malawi and implications for the biogeography of afromontane forests. J Biogeogr 25:479–500. https://doi.org/10.1046/j.1365-2699.1998.2530479.x
157. Dupont LM, Weinelt M (1996) Vegetation history of the savanna corridor between the Guinean and the Congolian rain forest during the last 150,000 years. Veg History Archaeobotany 5:273–292
158. Shi N, Schneider R, Beug HJ, Dupont LM (2001) Southeast trade wind variations during the last 135 kyr: evidence from pollen spectra in eastern South Atlantic sediments. Earth Planet Sci Lett 187:311–321. https://doi.org/10.1016/s0012-821x(01)00267-9
159. Phelps LN et al (2020) Asymmetric response of forest and grassy biomes to climate variability across the African Humid Period: influenced by anthropogenic disturbance? *Ecography* 43, 1118–1142 https://doi.org/10.1111/ecog.04990
160. Birks HJB, Line JM, Juggins S, Stevenson AC, Terbraak CJF (1990) Diatoms and PH reconstruction. Philosophical Trans Royal Soc B-Biological Sci 327:263–278. https://doi.org/10.1098/rstb.1990.0062
161. Terbraak CJF, Juggins S (1993) Weighted averaging partial least-squares regression (WA-PLS) - an improved method for reconstructing environmental variables from species assemblages. Hydrobiologia 269:485–502. https://doi.org/10.1007/bf00028046
162. Overpeck JT, Webb T, Prentice IC (1985) Quantitative interpretation of fossil pollen spectra - dissimilarity coefficients and the method of modern analogs. Quatern Res 23:87–108. https://doi.org/10.1016/0033-5894(85)90074-2
163. Breiman L (2001) Random forests. Mach Learn 45:5–32. https://doi.org/10.1023/a:1010933404324
164. De'ath G (2007) Boosted trees for ecological modeling and prediction. Ecology 88:243–251. https://doi.org/10.1890/0012-9658(2007)88[243:Btfema]2.0.Co;2
165. gbm: Generalized Boosted Regression Models (2019)
166. Liaw A, Wiener M (2002) Classification and Regression by randomForest. R News 2/3:18–22
167. rioja: Analysis of Quaternary Science Data (R package version 1.0–6 (2023)
168. R: A language and environment for statistical computing (R Foundation for Statistical Computing, Vienna, Austria (2022)

169. Gajewski K et al (2002) Modern climate-vegetation-pollen relations in Africa and adjacent areas. Q Sci Rev 21:1611–1631. https://doi.org/10.1016/s0277-3791(01)00152-4
170. Ivory SJ, Lezine A-M, Grimm E, Williams J (2020) Relaunching the African Pollen Database: Abrupt change in climate and ecosystems. Past Global Changes Magazine Past Plant Divers Conserv 28:26
171. Lezine A-M, Ivory SJ, Gosling WD, Scott L (2021) in *Quaternary Vegetation Dynamics* Ch. 2, 8CRC Press
172. Vincens A et al (2007) African pollen database inventory of tree and shrub pollen types. Rev Palaeobot Palynol 145:135–141. https://doi.org/10.1016/j.revpalbo.2006.09.004
173. Fick SE, Hijmans RJ (2017) WorldClim 2: new 1-km spatial resolution climate surfaces for global land areas. Int J Climatol 37:4302–4315. https://doi.org/10.1002/joc.5086
174. Hopcroft PO, Valdes PJ (2021) Paleoclimate-conditioning reveals a North Africa land-atmosphere tipping point. Proc Natl Acad Sci USA 118. https://doi.org/10.1073/pnas.2108783118
175. Pope VD, Gallani ML, Rowntree PR, Stratton RA (2000) The impact of new physical parametrizations in the Hadley Centre climate model: HadAM3. Clim Dyn 16:123–146. https://doi.org/10.1007/s003820050009
176. Gordon C et al (2000) The simulation of SST, sea ice extents and ocean heat transports in a version of the Hadley Centre coupled model without flux adjustments. Clim Dyn 16:147–168. https://doi.org/10.1007/s003820050010
177. Essery R, Best M, Cox PM (2001) Moses 2.2 technical documentation. Hadley Cent Tech note 30:1–30
178. Berger A, Loutre MF, Gallee H (1998) Sensitivity of the LLN climate model to the astronomical and CO < sub > 2 forcings over the last 200 ky. Clim Dyn 14:615–629. https://doi.org/10.1007/s003820050245
179. Loulergue L et al (2008) Orbital and millennial-scale features of atmospheric CH < sub > 4 over the past 800,000 years. Nature 453:383–386. https://doi.org/10.1038/nature06950
180. Spahni R et al (2005) Atmospheric methane and nitrous oxide of the late Pleistocene from Antarctic ice cores. Science 310:1317–1321. https://doi.org/10.1126/science.1120132
181. de Boer B, Lourens LJ, van de Wal RSW (2014) Persistent 400,000-year variability of Antarctic ice volume and the carbon cycle is revealed throughout the Plio-Pleistocene. Nat Commun 5. https://doi.org/10.1038/ncomms3999
182. The NCAR Command Language (2019) Version 6.6.2) [Software]. UCAR/NCAR/CISL/TDD, Boulder, Colorado.
183. Armstrong E, Valdes P, House J, Singarayer J (2017) Investigating the Impact of CO2 on Low-Frequency Variability of the AMOC in HadCM3. J Clim 30:7863–7883. https://doi.org/10.1175/jcli-d-16-0767.1
184. Ghil M (2002) Natural Climate Variability. John Wiley and Sons, Ltd.

185. Moron V, Vautard R, Ghil M (1998) Trends, interdecadal and interannual oscillations in global sea surface temperatures. Clim Dyn 14:545–569. https://doi.org/10.1007/s003820050241
186. Plaut G, Ghil M, Vautard R (1995) Interannual and interdecadal variability in 335 years of Central England temperatures. Science 268:710–713. https://doi.org/10.1126/science.268.5211.710
187. Peel MC, Finlayson BL, McMahon TA (2007) Updated world map of the Koppen-Geiger climate classification. Hydrol Earth Syst Sci 11:1633–1644. https://doi.org/10.5194/hess-11-1633-2007
188. Creese A, Washington RA, Process-Based (2018) Assessment of CMIP5 Rainfall in the Congo Basin: The September-November Rainy Season. J Clim 31:7417–7439. https://doi.org/10.1175/jcli-d-17-0818.1
189. Pokam WM, Djiotang LAT, Mkankam FK (2012) Atmospheric water vapor transport and recycling in Equatorial Central Africa through NCEP/NCAR reanalysis data. Clim Dyn 38:1715–1729. https://doi.org/10.1007/s00382-011-1242-7
190. Goñi MFS et al (2017) The ACER pollen and charcoal database: a global resource to document vegetation and fire response to abrupt climate changes during the last glacial period. Earth Syst Sci Data 9:679–695. https://doi.org/10.5194/essd-9-679-2017

Table 1

Table 1 is available in the Supplementary Files section.

Figures

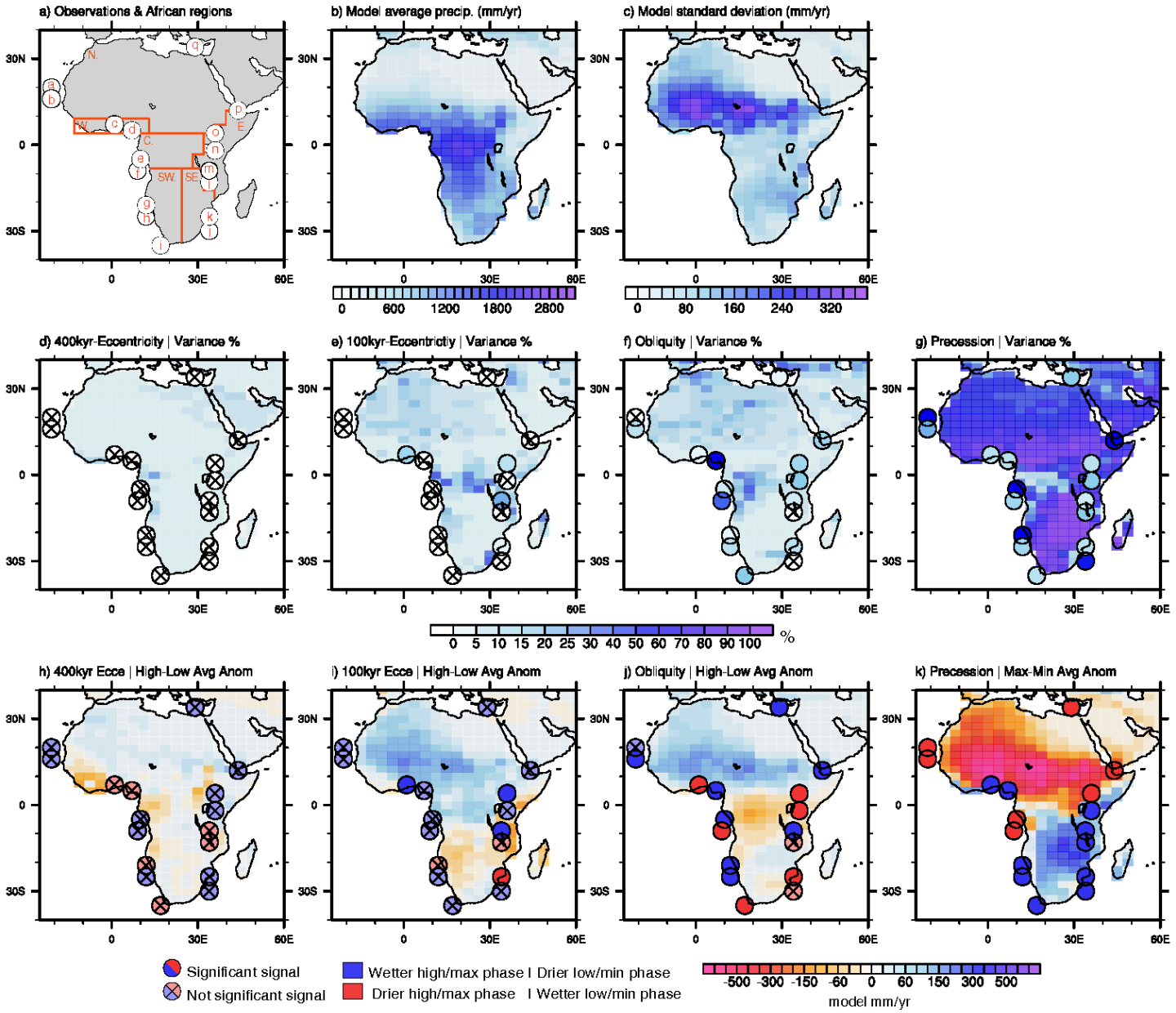

Figure 1

Analysis of orbital frequencies in the 17 hydroclimate proxies used in this study and the HadCM3BB-v1.0 modelled precipitation over the past 800kyrs. a) Location of proxies shown in Table 1 and Supplementary Figure 1 and boundaries of African regions discussed in the text and Methods, b) modelled annual average precipitation (mm/yr) (Methods), c) modelled precipitation standard deviation (mm/yr), d-g) variance contribution (%) of orbital frequencies to the overall variability in the model data (filled contour plot) and the detrended observation timeseries (filled circles) identified via singular spectrum analysis (SSA; Supplementary Figure 2, 5, Methods). Only observed orbital frequencies deemed 75% confident relative to a stochastic (Markov) process are shown (Methods). h-k) composite moisture anomalies for high/maximum – low/minimum orbital phases, where modelled anomalies (filled contours, mm/yr) are derived from the SSA-reconstructed orbital components, solid circles represent

proxies with 75% confident signals calculated from the orbital component timeseries, whereas crossed opaque circles are not confident proxy signals calculated from the raw proxy timeseries (see Methods). Orbital phases are defined in Supplementary Figure 3.

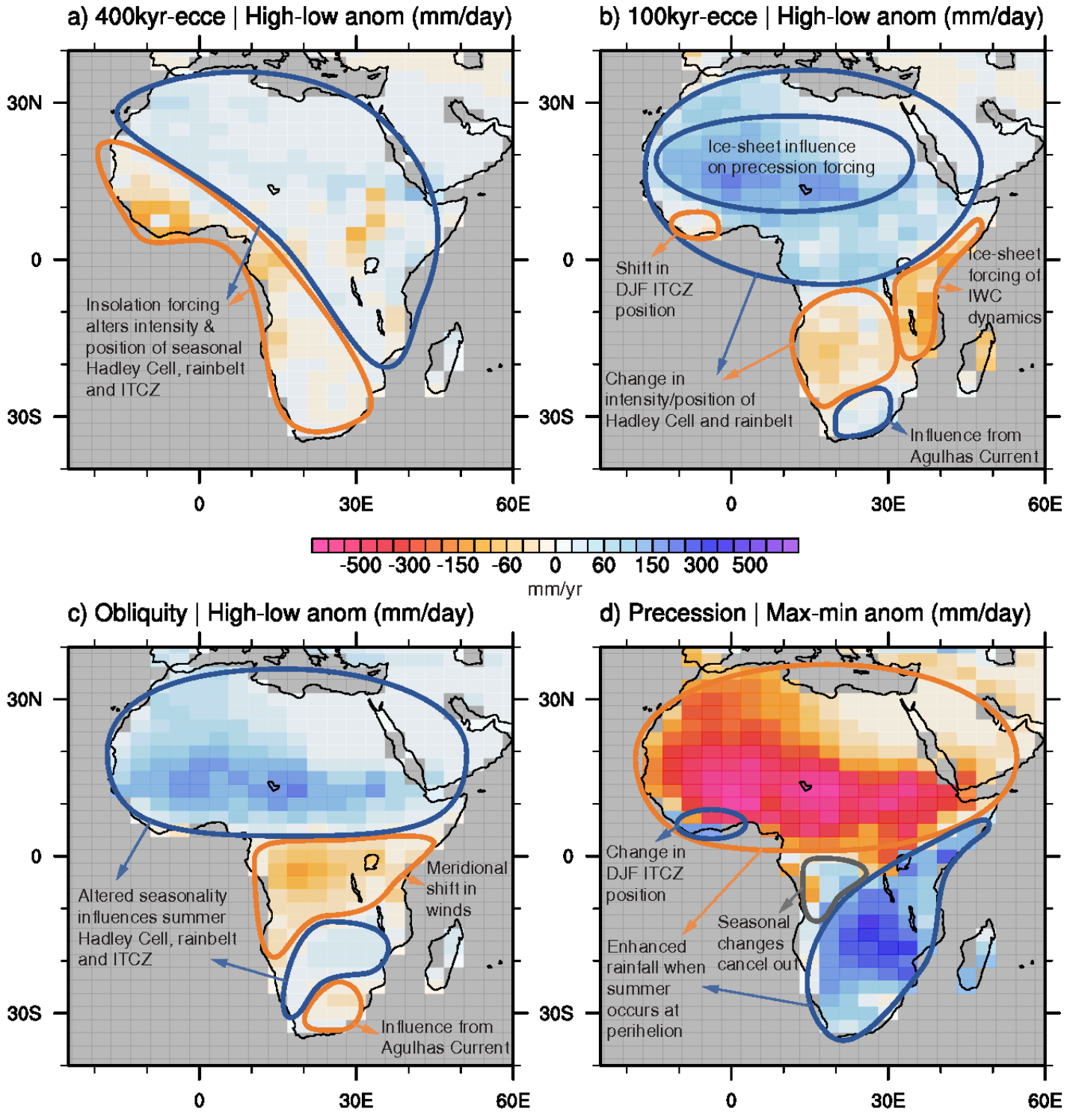

Figure 2

A summary of the modelled orbital forcing mechanisms for each orbital cycle shown with modelled (mm/yr) anomalies for high/max – low/min orbital phases (see Methods).

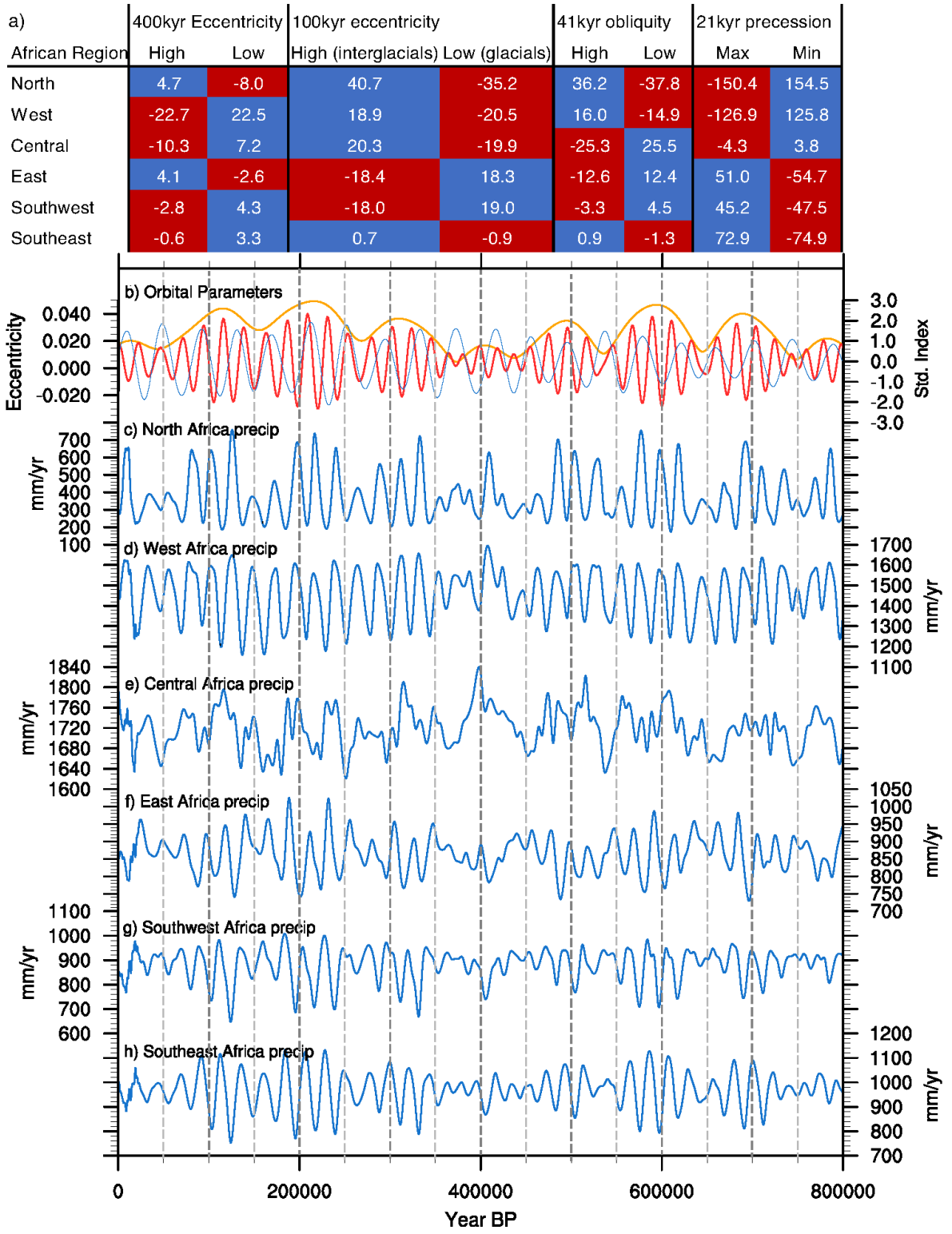

Figure 3

Regional average precipitation anomalies (mm/year) for each orbital cycle phase and timeseries of orbital parameters and regional precipitation timeseries (mm/yr). a) Regional anomalies for high/max-low/min orbital phases where blue (red) blocks indicate increased (decreased) average precipitation, and the numbers show the average modelled anomaly (mm/year). b) Orbital parameter timeseries with eccentricity (orange), obliquity (blue) and precession (red; with obliquity and precession on a

standardised index). c-h) Modelled regional precipitation timeseries (mm/yr) . African regions are defined in Figure 1a and the Methods. Orbital phases are defined in Supplementary Figure 3.

Supplementary Files

This is a list of supplementary files associated with this preprint. Click to download.

- SupplementaryInfoFinal.docx
- Table1SelectedObs.pdf